Morphostratigraphy of an active mixed sand–gravel barrier spit (Baie de Somme, Northern France)

Léo Pancrazzi, Pierre Weill, Bernadette Tessier, Sophie Le Bot, Laurent Benoît

SEDIMENTOLOGY the journal of the International Association of Sedimentologists

Sedimentology (2022) doi: 10.1111/sed.13018

Morphostratigraphy of an active mixed sand–gravel barrier spit (Baie de Somme, northern France)

LÉO PANCRAZZI*, PIERRE WEILL*, BERNADETTE TESSIER*, SOPHIE LE BOT† and LAURENT BENOIT*

**Normandie Université, UNICAEN, UNIROUEN, CNRS, M2C, 14000, Caen, France (E-mail: leo.pancrazzi@unicaen.fr)*

†Normandie Université, UNIROUEN, UNICAEN, CNRS, M2C, 76000, Rouen, France

Associate Editor – J.P. Walsh

ABSTRACT

This study focuses on the architectural characterization of a mixed sand-and-gravel spit in relation to its multi-decadal evolution. The spit, located in the Somme estuary in northern France, is a 5 km long sedimentary body made of several amalgamated ridges with a hooked terminus. Flint pebbles originating from the erosion of Cretaceous chalk cliffs and sands reworked from the tidal flat constitute the spit. Aerial photographs demonstrate that the spit formation started in the 1940s and document its growth through time. The architecture of the spit has been characterized by ground-penetrating radar (GPR) investigation using 400 MHz and 900 MHz antennas. The GPR data are used to distinguish progradational, aggradational and transgressive geometries that are related to cross-shore and longshore construction, respectively. Three main morpho-stratigraphic domains characterize the spit from the root to the terminus: (i) a beach-ridge domain mainly made of progradational structures; (ii) an intermediate domain formed by beach-drift structures topped by deposits with cross-shore geometries; and (iii) a spit-terminus domain mainly composed of beach drift structures which incorporate sand deposits. At the scale of an individual ridge, high-frequency GPR data indicates five types of sedimentary architectures associated with the evolution from a hook stage to the subsequent elongation stage. The overall development of the barrier spit is the result of complex interactions between wave and storm dynamics, potentially modulated by the variability of submersion time related to the 18.6 year tidal cycle, and anthropogenic activities including groyne construction and gravel reloading.

Keywords Barrier spit, English Channel, ground-penetrating radar, hypertidal, internal architecture, morphological evolution.

INTRODUCTION

Coastal spits are known for their high elongation rate due to littoral drift and their high preservation potential (Otvos, 2012). These coastal barriers are also sensitive to extreme marine events due to their narrow width and the lack of contact of their downdrift section with the mainland (Davidson-Arnott & Fisher, 1992). This study focuses on less studied gravel barriers that are closely related to energetic wave conditions and extreme storm events (Orford & Carter, 1982; Carter & Orford, 1984, 1993; Orford *et al.*, 2002; Orford & Anthony, 2011; Lindhorst & Schutter, 2014; Goslin & Clemmensen, 2017).

Coarse-grained barriers protect back-barrier environments from wave attack, as their steep beach face and very porous and permeable

sediment absorb wave energy and reduce wave run-up (Buscombe & Masselink, 2006). However, coarse-grained barriers, due to limited sediment sources, are more sensitive to variations in sediment supply as compared with their sandy counterparts (Orford *et al.,* 1991). Coarse sediment accumulations are related to various proximal sediment sources, including eroding cliffs (Carter & Orford, 1993; Isla & Bujalesky, 2000; Anthony, 2002; Letortu *et al.,* 2015), fluvial sediment supply (Massari & Parea, 1988; Dubar & Anthony, 1995), submarine platform erosion (Payo *et al.,* 2018), glacigenic sediment supply (Forbes *et al.,* 1995; Orford *et al.,* 2002) and biological sediment production (Holmes *et al.,* 2000; Etienne & Terry, 2012; Jahnert *et al.,* 2012; Weill *et al.,* 2012). Most coarse-grained barriers form in middle to high latitudes, with the exception of bioclastic barriers (shells, coral rubble). According to Jennings & Shulmeister (2002), gravel beaches can be classified based on grain-size distribution, and most are mixed systems composed of sand and gravel. Because grain size and sorting control sediment porosity and permeability, the degree of grain-size mixing between sand and gravel-size sediment controls swash–groundwater hydraulic exchange and consequently sediment transport (Buscombe & Masselink, 2006). For this reason, the degree of mixing has a strong influence on beach dynamics, and more generally on barrier behaviour. Earlier studies by Kirk (1975), Orford & Carter (1982) and Orford *et al.* (1991) have demonstrated the effects of a high permeability on swash and overwash dynamics, such as the rapid construction of berms and the smaller size of gravelly washover fans as compared with sandy fans. The emergence of high-resolution ground-penetrating radar (GPR) stratigraphy has provided new insight into the long-term evolution of such coastal bodies (Neal *et al.,* 2002; Jol & Bristow, 2003; Engels & Roberts, 2005; Montes *et al.,* 2018).

Barrier spits owe their characteristic morphologies to alternating phases of ridge elongation and of recurving that results in hook formation. However, the processes behind this alternation are still unclear. Some authors, such as Allard *et al.* (2008) and Poirier *et al.* (2017), support wave climate variability as a trigger for spit recurving, stating that spit elongation is more likely to be associated with energetic conditions and a high sediment flux rate, while hook creation is more likely to be associated with less energetic conditions and low sediment supply. Other authors support an autogenic control on these morphologies, such as spit-headland bypassing (Ashton *et al.,* 2016; Vieira da Silva *et al.,* 2016), inlet migration (Hayes, 1975; Tye & Moslow, 1993; Le Xuan *et al.,* 2011) or ridge stacking (Hine, 1979). The role of wave climate conditions in hypertidal environments, such as in the present study, is limited by the fact that wave action is not always effective on the spit (Kulkarni *et al.,* 2004; Robin *et al.,* 2009a). Tides do not directly affect hook formation but can control displacement of ebb delta swash bars across the estuary by intertidal channels (Robin & Levoy, 2007; Michel *et al.,* 2017) and modify the shoreline wave processes (Carter & Orford, 1984). The aim of this study is to investigate the sedimentary architecture of a coarse-grained barrier spit, in relation to its morphological evolution. The study, based on GPR investigation, focuses on a sand-and-gravel spit located at the mouth of the Somme estuary (English Channel, northern France). The spit started to form in the 1940s and has undergone rapid development. Its evolution is well-documented by aerial photographs, which provide useful chronological markers if linked to the GPR stratigraphy. This combined approach provides new keys to better understand the morphodynamic processes that control internal structure and development of gravel spits, such as longshore versus cross-shore construction and formation of a hooked terminus.

STUDY AREA

The study area is located along the southern shore of the Baie de Somme (northern France), the main estuary of the northern English Channel. The Baie de Somme, including supratidal and intertidal areas, covers a 70 km^2 area (Fig. 1A and B). The internal bay and sheltered areas are dominantly composed of salt marshes and mud flats incised by tidal creeks. Together with the main channels of the Somme and the Maye rivers, tidal channels form a complex network in the sandy intertidal domain that progressively widen seaward. This channel-and-shoal intertidal zone extends offshore through a 5 km wide inlet, forming a vast and almost symmetrical ebb-tidal delta. To the north, the inlet is bordered by ancient Pleistocene sand spits and dunes sheltering a partially reclaimed coastal plain (Marquenterre and Le Crotoy areas; Fig. 1). The southern side of the inlet is characterized by a 16 km long gravel barrier spit (the Cayeux spit) extending from its root at Ault-

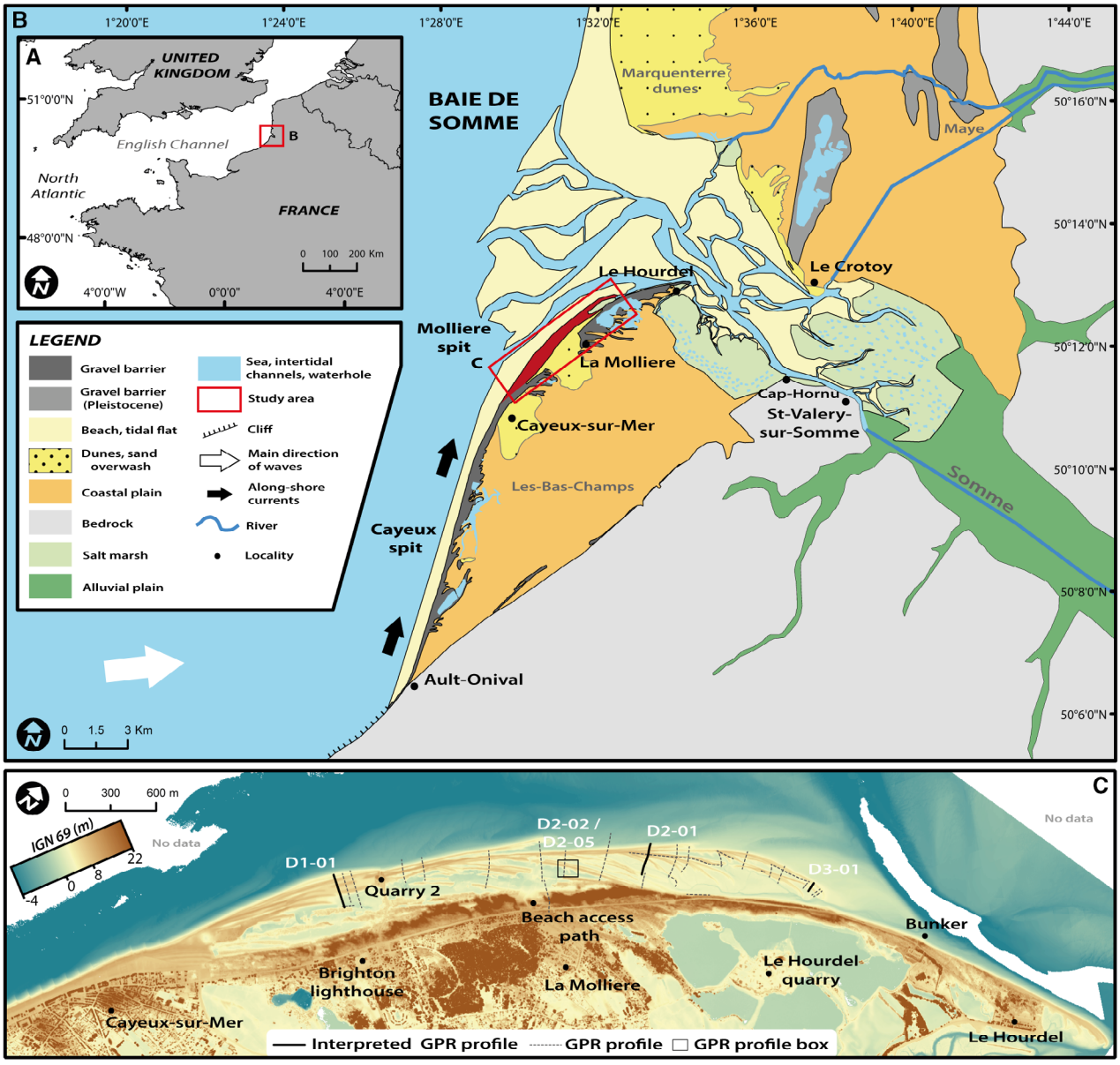

Fig. 1. (A) Location map of the study area (coordinates in WGS84). (B) Morpho-sedimentary map of the Baie de Somme. (C) Location of the GPR profiles at the Mollière barrier spit. Background digital elevation model (DEM) derived from 2017 LiDAR data – IGN 69 elevation datum (ROL, Réseau d'Observation du Littoral). Mean sea-level = 1.106 m IGN.

Onival, to its terminus at Le Hourdel (Fig. 1). The construction of the Cayeux spit began at the foot of a Cretaceous cliff at Ault-Onival, about 2500 years ago (Dupont, 1981). As the spit elongated northward under the action of the regional dominant littoral drift, it progressively deviated from the cliff, with low sheltered wetlands developing between the newly formed barrier and the fossil cliff. These wetlands now cover an area of 43 km^2, and were reclaimed during the 17th and 18th centuries and called 'Les-Bas-Champs' (Fig. 1). The wetlands' average elevation is 4 to 5 m below the highest tide level.

The main pebble source of the barrier is from the retreat of the coastal cliffs composed of Cretaceous chalk with flints (Colbeaux *et al.*, 1980), located south of Ault-Onival. Cliff erosion delivers flint pebbles that are transported northward by littoral drift (Costa, 1997). Pebble size ranges between 3 cm and 7 cm.

The Baie de Somme experiences a semi-diurnal hypertidal regime (Archer, 2013) with a mean tidal range of 8.65 m in front of the barrier. Water levels during mean neap and spring tides reach 3.56 m IGN and 5.41 m IGN (French elevation datum, mean sea-level = +1.106 m IGN), respectively. The highest astronomical tides (HAT) reach 6.14 m IGN (SHOM, 2017). Surface tidal currents measured at the spit terminus (i.e. at Le Hourdel in the estuarine inlet) reach up to 2.5 m s^{-1} during spring tide flood (SOGREAH, 1995, in Michel, 2016). Dominant winds blow from west to south-west and produce offshore waves that are typically <2 m high and approach from the same sector. Offshore waves >4 m high and with a period higher than 8.5 s are occasionally measured (Bastide, 2011). This west/south-west wave dynamic generates the dominant northward littoral drift and the longshore transport of flint pebbles. The mean elevation of the barrier is 8.0 to 8.5 m IGN, i.e. about 2 m above the highest tide levels. In this area, decennial, centennial and millennial surges are at 0.91 m, 1.32 m and 1.76 m with regard to mean spring tide level (Bastide, 2011).

The overall evolution of the Cayeux spit during the last decades is documented in aerial photographs and historical maps. Examination of this material indicates that: (i) the downdrift elongation of the barrier is negligible, with the spit terminus (Le Hourdel) being reworked by the wandering of tidal channels at the inlet; (ii) south of Cayeux-sur-Mer, the retreating barrier has been largely restored by beach nourishment and installation of >100 groynes over 10 km of the coast; and (iii) the only sector prograding along the barrier is located between Cayeux-sur-Mer and the quarry of Le Hourdel (Fig. 1), where a 5 km long gravel spit (hereinafter referred as the Mollière spit, in red in Fig. 1) developed along the larger Cayeux spit since the 1950s (Dolique & Anthony, 1999; Bastide, 2011). Because its recent development can be monitored by aerial photographs, the Mollière spit has been chosen to investigate the detailed morphostratigraphy of a gravel spit.

METHODOLOGY

Aerial images

The oldest aerial photograph of the study area is from 1935 CE. From 1940 to 2000 CE, approximately one aerial image per decade is available (BD ORTHO® Historique, IGN, Institut Géographique National). Five additional infrared aerial photographs, with a horizontal accuracy of ±0.5 m, are available within this time span (1961 CE, 1975 CE, 1986 CE, 1997 CE and 1999 CE). They provide complementary information with higher contrast between sand and gravel deposits. After 2000 CE, five images per decade can be used thanks to additional Pleiades (±0.5 m, IGN) and SPOT (±1.5 m) data. Two LiDAR surveys in 2013 CE and 2017 CE (ROL, Réseau d'Observation du Littoral) are also available, providing accurate elevation data of the barrier spit.

Image georeferencing has been performed using QGIS 3.6 (QGIS Development Team, 2019). Geodesic system RGF93 with IAG-GRS80 was chosen as the reference ellipsoid and Lambert93 conic as the projection system with metric coordinates.

The Mollière spit has been mapped and digitized on all available images. The main criteria to digitize each ridge were the colour and textural contrast between sand and gravel deposits. These data allowed for highlighting of the cross-shore and longshore evolution of the barrier spit system since the beginning of its construction. Additionally, the position of the crest of the active ridge in every image provides chronological markers traced into the GPR profiles.

Ground-penetrating radar

Ground-penetrating radar (GPR) has been widely used in coastal environments (e.g. Neal *et al.,* 2002; Jol & Bristow, 2003; Engels & Roberts, 2005; Lindhorst *et al.,* 2008; Tamura *et al.,* 2008; Bennett *et al.,* 2009; Jahnert *et al.,* 2012; Tamura, 2012; Weill *et al.,* 2012; Tillmann & Wunderlich, 2013; Billy *et al.,* 2014; Fruergaard *et al.,* 2015, 2020; Baumann *et al.,* 2017; Montes *et al.,* 2018). The main limitation of GPR is the dissipation of the electromagnetic signal in highly conductive sediments, such as beach sands saturated with saltwater, and mud-dominated deposits (Leatherman, 1987; Jol *et al.,* 1996; van Heteren *et al.,* 1996, 1998). By contrast, GPR usually provides high-quality data in granular coastal sediments lying above the saltwater table, such as upper beaches, washover deposits and aeolian dunes, with penetration depth in the order of a few metres to 10 m.

In the present study, the GPR survey was carried out using a GPR SIR-3000 system (Geophysical Survey Systems, Inc., Nashua, NH, USA)

with 400 MHz and 900 MHz shielded antennas. The 400 MHz antenna was used for the large-scale survey of the spit along shore-normal transects, complemented locally by shore-parallel profiles. The 900 MHz antenna was used to more accurately image specific parts of the barrier, such as spit hooks or washover lobes. Although the GPR survey was performed during low neap tide, when the gravel spit had not been flooded for several days, the sand platform below the gravel barrier was still saturated with seawater. Mean signal penetration depth reached up to 5 m with the 400 MHz antenna and never went below 2 m IGN, which is approximately the elevation of the intertidal sand platform. As a result, penetration of the active beach face was strongly limited and was almost null in the topographic lows and the back-barrier system, due to the presence of clayey sediment and the nearly outcropping saltwater table. Ground-truthing with cores or trenches was not possible due to the very coarse nature of the sediment. In parallel to GPR data acquisition, high-resolution topographic data were acquired using a DGPS Leica Viva GNSS GS10 (Leica Geosystems AG, Heerbrugg, Switzerland) with 2 cm vertical accuracy. A total of 6 km of GPR profiles were acquired along the barrier, from the root to the terminus of the spit (Fig. 1C).

The GRPGy software (Plattner, 2020) was used to process the GPR data, including time-zero adjustment, background removal, time-depth conversion, migration (f-k Stolt) and topographic correction. For time-to-depth correction, a velocity of 0.112 m ns^{-1} was chosen based on the analysis of reflection hyperbolas (Jol & Bristow, 2003). This value is consistent with the velocity range in unsaturated sand and gravel deposits provided by Neal & Roberts (2000) and Neal (2004). DGPS data has been used for the topographic correction of the profiles.

RESULTS AND STRATIGRAPHIC INTERPRETATIONS

Morphological evolution of the Mollière spit

In 1935 CE, three gravel ridges formed the incipient 1 km long Mollière spit between Cayeux-sur-Mer and the lighthouse of Brighton [Fig. 2, 1935 CE (1)]. A few hundred metres down-drift of the small Mollière spit terminus, the coastline of the large Cayeux spit appeared sandy. The intertidal platform was covered by well-developed sandy swash bars [Fig. 2, 1935 CE (2)].

From 1939 CE, the Mollière spit started to develop across the area later mapped with GPR. Gravel ridges started to appear from the south-west on the 1947 CE image [Fig. 2, 1947 CE (1)]. To the north-east, sandy swash bars merged on the upper tidal flat. Attached to the coastline, at an inflection point [Fig. 2, 1947 CE (2)], this sandy platform isolated a small depression behind [Fig. 2, 1947 CE (3)]. By 1961 CE, the first gravel ridge that had appeared on the 1947 CE image had grown <200 m eastward and displayed a well-defined hooked termination, almost attached to the shore [Fig. 2, 1961 CE (1)]. It is succeeded by a set of at least four elongated ridges [Fig. 2, 1961 CE (2)], which led to the overall elongation of the Mollière spit by about 700 m. The development of this new set led to the progradation of the coastline of about 250 m. The individual ridges have an arcuate shape and are re-attached to the shore on their downdrift termination. The elongation of the younger ridge continued behind its re-attachment point, growing quickly on a likely sandy platform. Downdrift of the coastline inflection point [Fig. 2, 1961 CE (3)], the sandy platform prograded seaward, associated with the amalgamation of large sandy swash bars [Fig. 2, 1961 CE (4)]. Until 1991 CE the spit was moderately reshaped and elongated by the addition of a few new ridges, the distal terminations of which are attached to the main shore [Fig. 2, 1991 CE (1)]. Spit elongation was about 1000 m in 30 years. Between 1991 CE and 2000 CE (<10 years) a new set of ridges of about the same size as the previous one has developed [Fig. 2, 2000 CE (1)]. The construction of a sandy platform by swash-bar amalgamation appears to be an important process for gravel spit elongation. Individual ridges at the spit end are less amalgamated and shorter than they were before 2000 CE. Most of the distal ridge extremities are not attached to the main shore, displaying a free hooked termination. This third set continued spit elongation until the present with the addition of new very long ridges (about 600 m) [Fig. 2, 2013 CE (1)]. The total spit elongation from the 1930s to the present is about 5 km, with a maximum coastline progradation of about 300 m. A wide salt marsh area developed between the active Mollière spit and the main coastline of the Cayeux spit. In the most recent image (2017 CE) two new ridges of about 120 m and 300 m in length appear in front of the previously described ridge sets [Fig. 2, 2017 CE (1,2)].

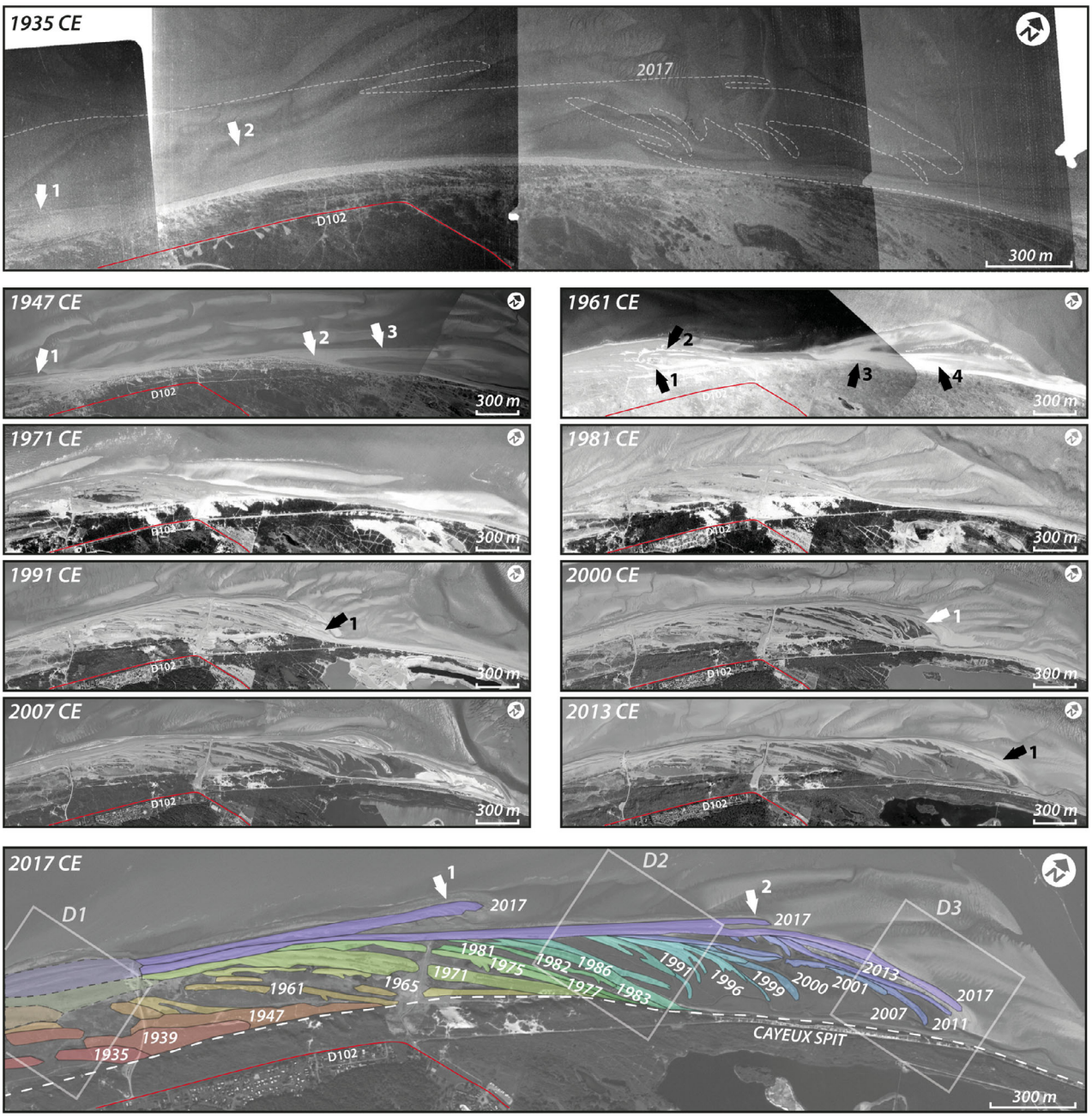

Fig. 2. Main evolutionary stages of the Mollière spit since 1935 CE based on analysis of aerial photographs (from 1935 to 2013 CE) and satellite imagery (Spot, 2017 CE). Ridge chronology and the location of domains D1, D2 and D3 (Fig. 3) are presented on the 2017 CE image. Road D102 is highlighted in red to help comparisons between images. Arrows highlight morphological features that are described in the text.

Finally, image analysis shows that almost all of the structures that formed during the 70-year evolution of the Mollière spit have been preserved (Fig. 2, 2017 CE). From this analysis, the Mollière barrier spit can be subdivided into three main morpho-sedimentary domains from the south-west to the north-east (Fig. 3; locations on Fig. 2), termed D1 to D3. The root domain (D1) is characterized by a wide gravel barrier made of ridges amalgamated since the 1960s (Figs 2 and 3). D1 essentially shows seaward beach-ridge-like progradation. The terminations of ridges developed prior to 1960 CE are isolated behind D1. The intermediate

domain (D2) is composed of the ridges that developed between 1961 CE and 1986 CE. These ridges are all re-attached to the main Cayeux spit. The Mollière spit terminus domain (D3) corresponds to the last elongation stage of the spit which occurred since 1991 CE. Individual ridges in D3 are not re-attached to the main Cayeux spit and display a hooked termination.

Descriptions and interpretations of GPR facies and geometries

Seven main radar facies have been distinguished based on amplitude, geometry and continuity of reflections (Fig. 4). The combination of radar facies and delimiting radar surfaces allows delimination of sedimentary bodies, which are interpreted in terms of depositional processes, and which are classified as progradational, aggradational or overwash features.

The main characteristics of the radar facies in terms of reflection geometries are included in Fig. 4. The following section interprets the seven facies based on these characteristics. Facies F1 is observed on the seaward face of individual ridges and is thus related to swash deposits, which constitute the beach face (main progradational domain). F1 on active ridges is abruptly attenuated by the presence of saltwater in the sediment (Facies F1'). Radar facies F2 represents aggradational berm geometries. Facies F3 forms the core of individual ridges in the intermediate and terminus domains D2 and D3 and is not observed above the highest tide levels. Facies F4 is interpreted to characterize washover deposits. Washover deposits are underlain by erosive surfaces and constitute aggradational sedimentary units. Facies F5 is associated with overtopping deposits, which contribute to ridge aggradation, and fits on the top of ridges (crests). Facies F6 is visible on the landward side of the ridges within the morpho-sedimentary domain D3 and is characteristic for aeolian sand dunes. Facies F7 is commonly observed on salt marshes located behind D2 and D3 ridges. Here, signal attenuation and low penetration depth are associated with the conductive inter-ridge sediments, made of silt and clay partially saturated by brackish to salty water.

Internal architecture of the Mollière spit

Three GPR profiles are used to illustrate the three morpho-sedimentary domains of the Mollière spit (root – D1, intermediate – D2 and terminus – D3).

Root domain (D1). The internal architecture of the root domain (D1) is illustrated by GPR line D1-01 (Fig. 5), a 220 m long cross-shore profile. Line D1-01 starts at the limit between the sandy tidal flat and the gravel beach face, at an elevation of 4 m IGN. Its landward termination is located in a flat, dry and sandy back-barrier depression at 4 to 5 m IGN. The prominent gravel barrier, with an elevation of 7 to 8 m IGN, is situated on the profile between the 20 m and 140 m distance markers. It is topographically characterized by three ridges decreasing slightly in elevation landward (Fig. 5A) separated by 1 m deep depressions. The active beach-face slope angle is 5 to 9° below the high spring tide (HST) level (5.41 m) and is more than 17° above the HST level. The landward slope of the barrier is about 5°.

Signal penetration is variable along the profile, from: (i) a few tens of centimetres on the active beach face (profile distance 0 to 15 m; Fig. 5A to C); (ii) 3 to 4 m below the seaward ridge; (iii) to about 5 m in the two landward ridges (50 to 125 m); and (iv) around 3 m in the back-barrier flat (150 to 220 m). Primary, high-amplitude and continuous reflections bound sedimentary bodies of various geometries including beach-face deposits (radar facies F1; compare Fig. 4), berms (F2), washover lobes (F4) and overtopping deposits (F5). These sedimentary bodies have been classified in terms of aggradational, progradational or transgressive units, and numbered from 0 to 29 based on their stratigraphic chronology (Fig. 5C). According to their stacking patterns, the radar units can be grouped into Unit Sets (US). Within the root domain (D1), four Unit Sets (USr1 to USr4) are distinguished as follows, from the oldest to the youngest.

- USr1 (units 0 to 7) is essentially composed of beach-face deposits (F1), associated with a shoreline progradation on 60 m. The lowermost units are flat-lying whereas slope values are maximum (up to 6°) within the uppermost units. The top of the Unit Set rests at 4 m IGN, which is the current sand-flat elevation. It is likely that the low-elevation of USr1 is the consequence of gravel pits as suggested by truncated gravel ridges observable on the LiDAR DEM.
- USr2 (units 8 to 15) is associated with a strong aggradation (F5) of the barrier (more than

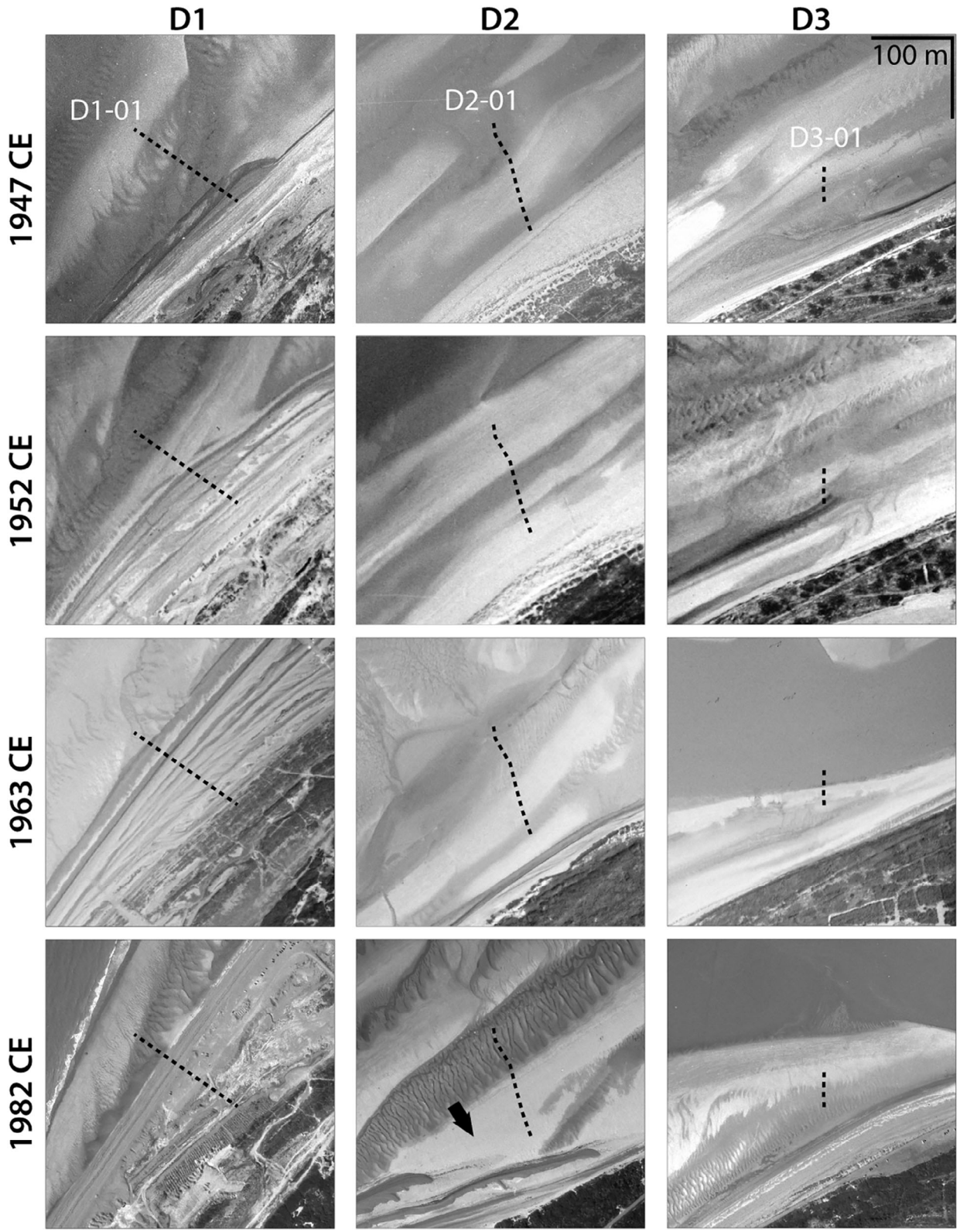

Fig. 3. Temporal evolution of the three morpho-sedimentary domains illustrated by aerial photographs (from 1947 to 2017 CE). All images have the same geographic footprint (located in Fig. 2–2017 CE). GPR lines D1-01, D2-01 and D3-03 shown in Figs 5 to 7 are indicated in each domain. Arrows highlight morphological features that are described in the text.

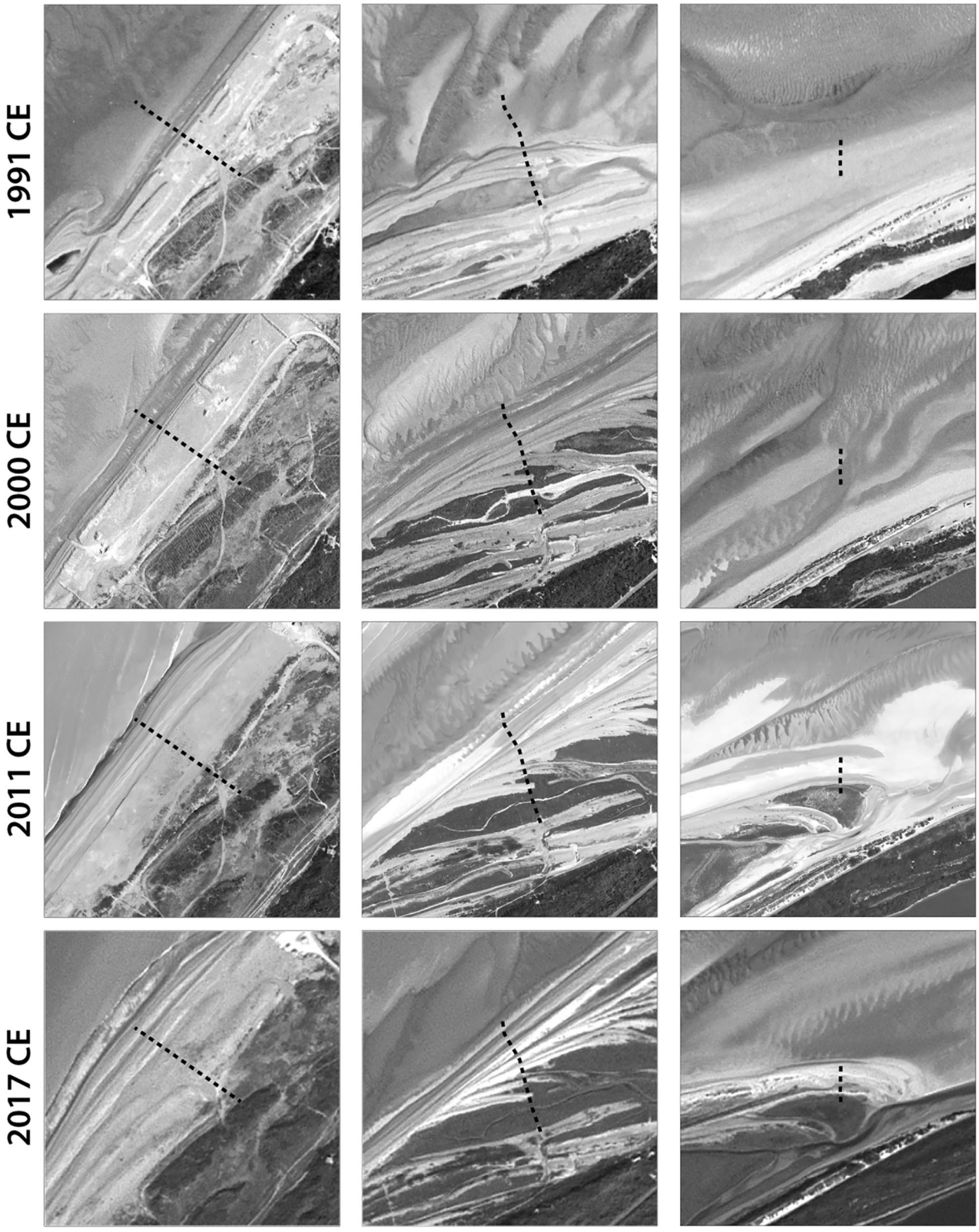

Fig. 3. Continued

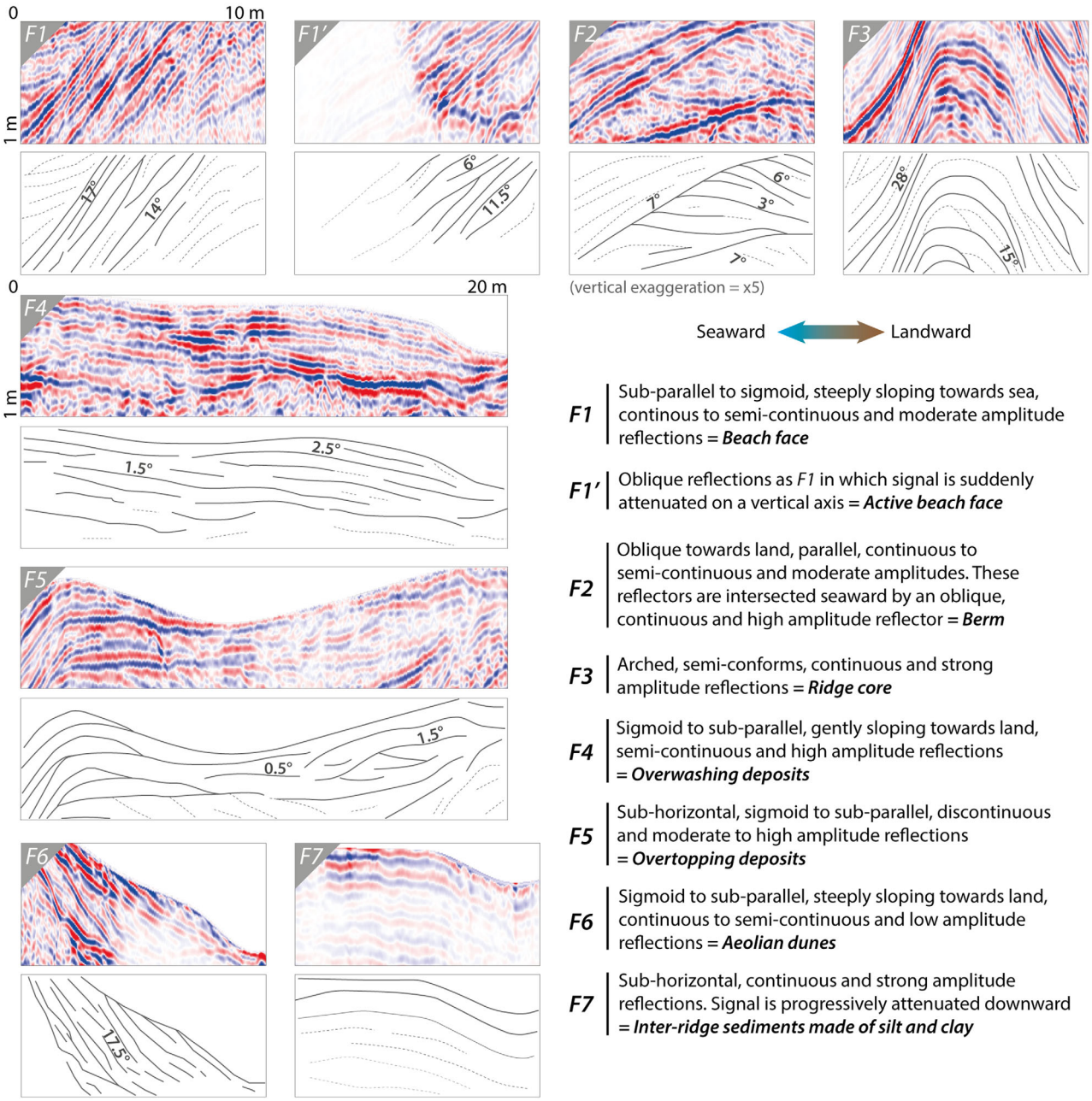

Fig. 4. Radar facies defined from GPR profiles. All image samples are extracted from cross-shore profiles (sea to the left).

2 m), by the top of unit 15 reaching the highest tide level. The overall progradation of USr2 is about 40 m.

- USr3 (units 16 to 23) comprises almost exclusively progradational beach-face deposits (F1). The progradation of USr3 occurred over a distance of 50 m. A slight aggradational component approximately 1 m thick is associated with units 22 and 23, which reaches an elevation of 7.5 m IGN. The base of the bottom sets, when visible, is at around 4 m IGN.
- USr4 (units 24 to 29) forms the youngest ridge, anchored on a nucleus associated with units 24 and 25. Berm deposits (F2) allow the ridge aggradation and the progradation of beach-face deposits (F1). Berm and beach-face deposits are sometimes reworked as washover deposits (F4). The top of USr4 reaches an elevation of 8 m IGN, almost 2 m above the highest tide level.

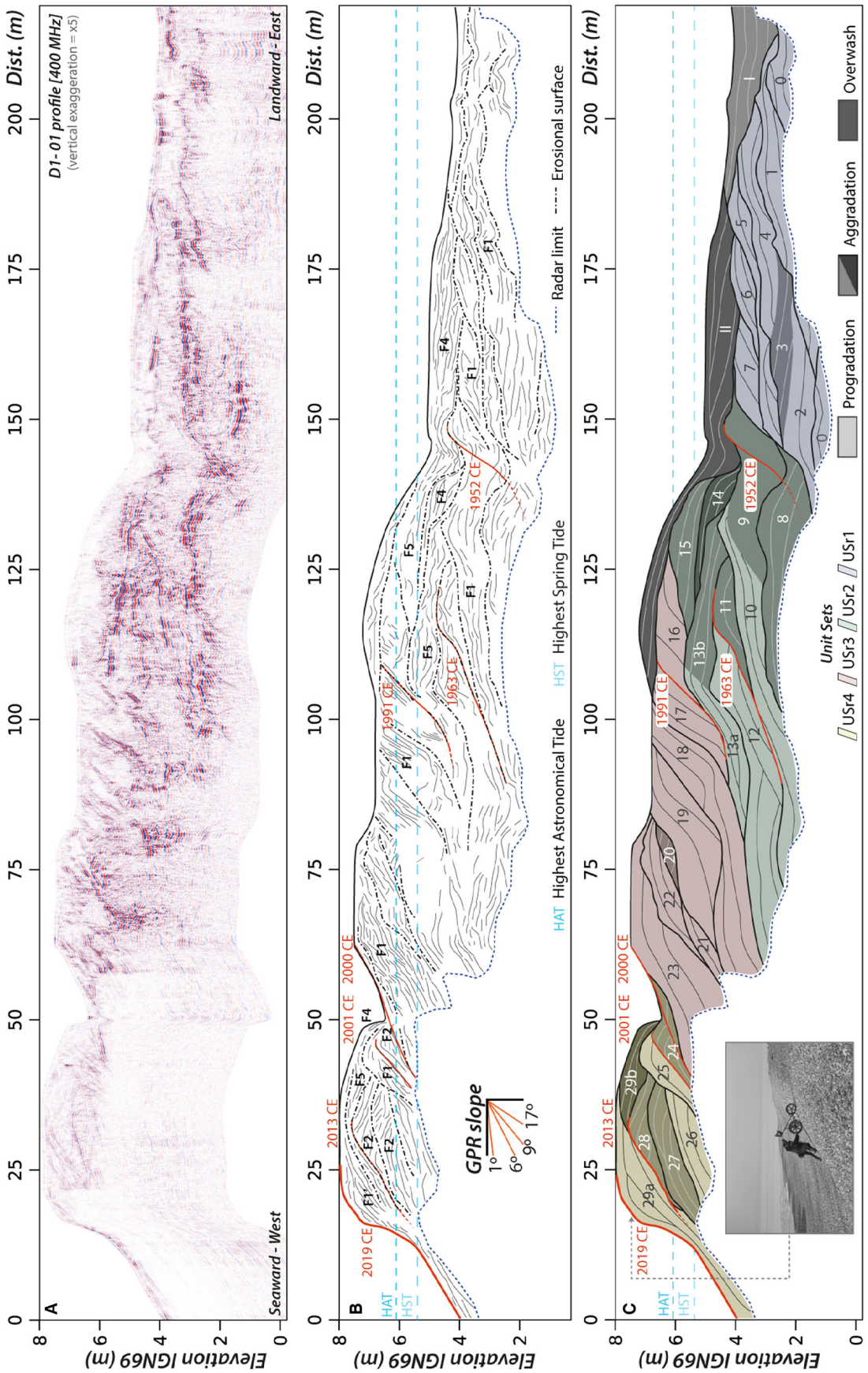

Fig. 5. D1-01 GPR profile interpretation in the root domain D1. (A) GPR data. (B) Line drawing. (C) Interpretation with unit numbers (sedimentary bodies) numbers, stacking pattern and Unit Sets numbers (USr).

Two additional units (I and II) have been identified, although their chronostratigraphical relationship remains unclear. Unit I onlaps the landward side of USr1, at an elevation ranging between 3 m IGN and 4 m IGN. The purely aggradational geometry suggests that unit I is the result of the infilling of the back-barrier depression, probably during tidal inundation. Unit II shows overtop–overwash geometries. It partly overlaps USr3 and completely overlaps USr2, and downlaps the top of USr1. Unit II results from overwashing processes during the deposition of USr3 past 1991 CE.

Seven time-lines between 1952 CE and 2019 CE are identified within the GPR line using the aerial and satellite images (Fig. 5B and C). According to these markers, the chronological frame of the successive Unit Sets can be proposed: USr1 (dominant progradation) before 1952 CE; USr2 (dominant aggradation) between 1952 CE and the 1980s; USr3 (dominant progradation) during the 1990s; and USr4 (the last ridge, mixed progradation/aggradation) during the last 20 years. The overall evolution from USr1 to USr4 is a continuous progradation combined with general aggradation.

Intermediate domain (D2). The internal architecture of the intermediate domain (D2) is imaged by the GPR line D2-01 (Fig. 6), a 210 m long cross-shore profile. It starts at the limit between the sandy tidal flat and the gravel beach face, at an elevation of 3 m IGN. Its landward termination is located at 6 m IGN at the foot of a fossilized ridge (Fig. 6A and B). The first 40 m of the profile correspond to the active ridge, with a steep beach-face slope (12°) and a crest reaching almost 7 m IGN. Between 40 m and 120 m, a sequence of four stacked ridges developed, their crest at 7 to 8 m IGN being clearly visible, separated by troughs, more than 1 m deep. A 15 m wide and 2 m high ridge occurs at 135 m, and it is isolated from the previously described ridge cluster by fine-grained back-barrier deposits. Finally, a 60 m wide salt-marsh extends up to the end of the GPR profile. It has an elevation of 4.5 m IGN and is incised at 160 m by a small tidal creek (Fig. 6A).

The maximum signal penetration depth is around 3 m under the main ridges. It decreases towards the active beach. As for GPR profile D1-01 within the spit root domain (D1), radar units are numbered, based on their stratigraphic chronology, from 0 to 23 (Fig. 6C), and grouped into three Unit Sets (USi1 to USi3).

- USi1 (units 0 to 9) comprises three individual ridges. They are composed of an aggradational ridge core (F3 – units 1, 4 and 7), flanked seaward and landward by a progradational beach-face (F1 – units 0, 2 and 5) and overwash deposits (F4 – units 3 and 6), respectively. Unit I, which has been deposited after the gravel ridges, corresponds to salt marsh deposits (F7) between ridges.
- USi2 (units 10 to 18) comprises three ridges. Aggradational ridge core deposits (F4 – units 10b, 10c, 14 and 16) are set on gently seaward-dipping surfaces, possibly lower beach-face deposits (unit 8) or low-lying sediment bodies, such as sand bars that develop in front of gravel ridge terminations (units 11 and 12). The height of the aggradational ridge core never exceeds the highest tide level. These cores are flanked seaward and landward by progradational beach-face deposits (F1) and overtopping deposits (F5) to washover deposits (F4), respectively. Because of overtopping, the ridge crests reach an elevation between 7 m IGN and 8 m IGN. Due to their proximity, the ridges are strongly amalgamated; overwash deposits of the most seaward ridge fill the inter-ridge depression and progressively onlap the beach-face deposits of the ridge landward.
- USi3 (units 19 to 23) comprises the two youngest ridges, built by an aggradational ridge core (F3 – unit 20), topped by overtopping and washover deposits (F4/F5 – units 21 and 22b), which partly lean on USi2, and beach-face deposits (F1 – unit 22a). Unit 23 is the active beach face (F1').

As for the spit root D1, five time-lines between 1991 CE and 2019 CE have been placed along the GPR profile of the intermediate domain D2. The following chronological frame of the Unit Sets is proposed: USi1 (dominant aggradation) before the middle of the 1990s; USi2 (mixed progradation/aggradation/transgression) between the middle of the 1990s and the middle of the 2000s; and USi3 (mixed progradation/aggradation) during the last decade. Unit I is still activated at present by tidal channels.

Terminus domain (D3). The internal architecture of the spit terminus (D3) is imaged by the 60 m long cross-shore GPR profile D3-01 (Fig. 7). The GPR line starts on the active beach face, crosses two gravel ridges, and ends in the back barrier salt marsh. The mean signal penetration depth is 4 m, except on the active beach face and salt marshes where the signal is

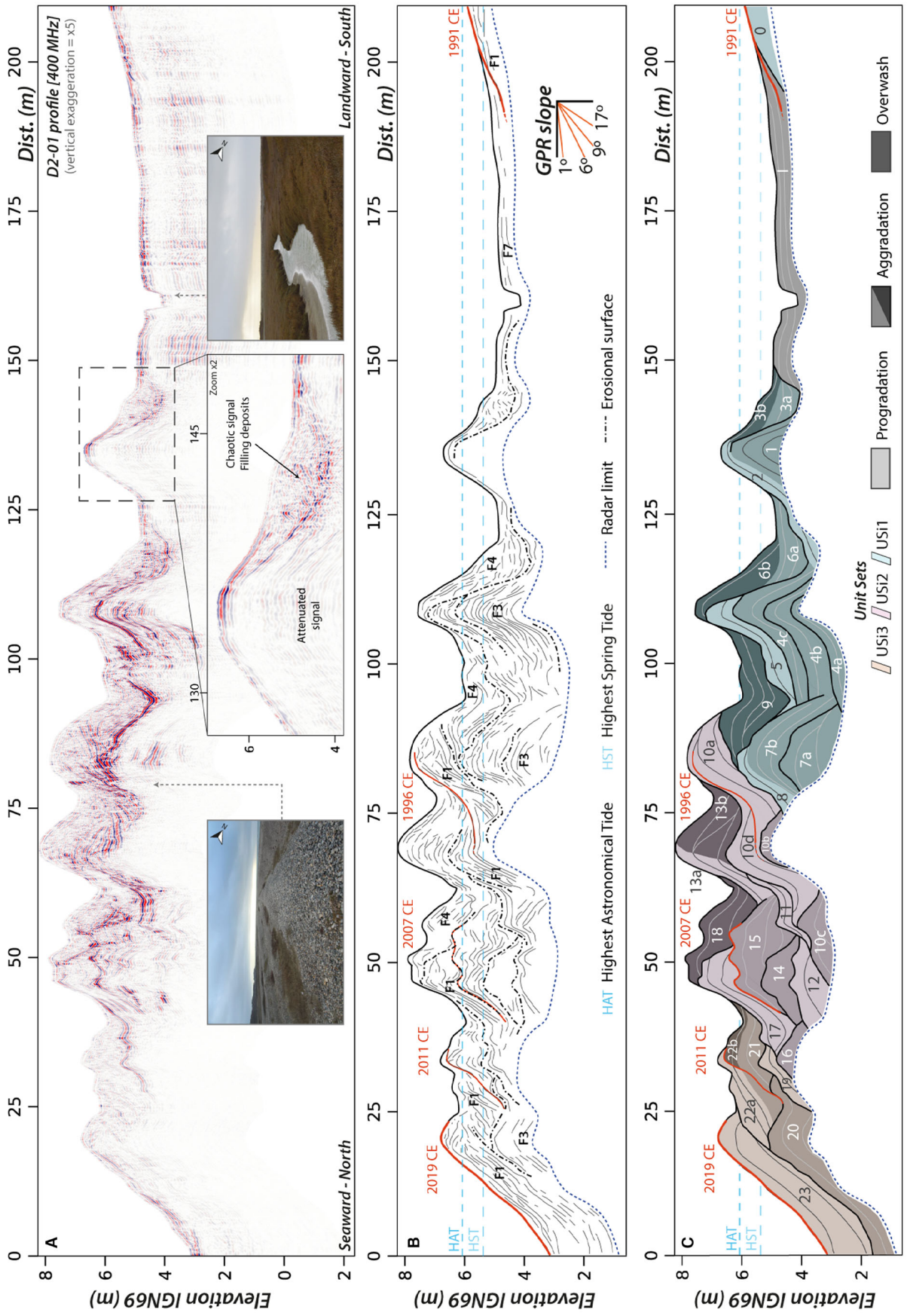

Fig. 6. D2-01 GPR profile interpretation in the intermediate domain D2. (A) GPR data. (B) Line drawing. (C) Interpretation with unit numbers (sedimentary bodies), stacking pattern and Unit Sets numbers (USi).

strongly attenuated. The ridge crests are elevated above the highest tide level (6.3 m IGN and 7.1 m IGN) and frame a small inter-ridge depression. The main radar surfaces allow distinguishing three main Unit Sets (USt1 to USt3).

- USt1 is composed of unit 0 which is a 2 m thick aggradational sequence at the base of the barrier. It shows discontinuous, conform, sub-horizontal to gently seaward-dipping reflections. The erosional top surface is dipping seaward with an angle between 1° and 2°.
- USt2 (unit 1 to 4) unconformably overlays USt1. USt2 is composed of aggrading sediment packages. These form the basement of the two ridges, which frame a 20 m wide and 1 m deep depression filled with washover deposits (F4 – unit 4a) and aggrading deposits (unit 4b). The top of USt2 is bound by an erosional surface dipping seaward with an angle of 1°.
- USt3 (units 5 to 8) corresponds to the development of the two ridges above HST level. The most landward ridge, located 1 m above the highest tide level, is composed mainly of beach-face deposits (F1– unit 7), backed by aeolian dunes (F6 – unit 8). The youngest ridge, barely above the highest tide level, shows a gently seaward-dipping beach face (F1 – unit 6a) backed by washover deposits (F4 – unit 6b).

Since the evolution of the spit terminus domain (D3) is dominantly aggradational, timelines based on aerial image analysis apply only to USt3. Time markers allow the inner ridge to be dated to 2011 CE (the seaward is the present-day ridge). Throughout the domain aggradational geometries were only deposited below the highest tide level, as suggested by the unusually low-angle dipping slope, if compared to the two previous morpho-sedimentary domains (D1 and D2).

Hook structures and connecting points

A hooked ridge terminus has been surveyed in detail using a 900 MHz antenna and closely-spaced orthogonal profiles for a high-frequency GPR investigation (Fig. 8A, see location in Fig. 1C).

Main ridge

D2-02 is a 70 m long shore-parallel profile that follows the crest of the main ridge (Fig. 8B). Signal penetration is about 3.5 m and allows the distinction of four units (1 to 4, Fig. 8B'). Unit 1 is a basal unit located updrift of the hook inflection point (Fig. 8A). It is characterized by oblique, continuous reflections of moderate amplitude which are downlapping on a horizontal reflection at 4.5 m IGN. Unit 2, located between 40 m and 70 m, is a basal unit located downdrift of the hook inflection point. It is bounded at the base by the same horizontal reflection as unit 1 and at the top by a continuous and sub-horizontal reflection at 5.5 m IGN. Both units are located below HST, and the transition between unit 1 and unit 2 corresponds to the position of the hook inflection point [Fig. 8B' (I1)]. Unit 3 covers the two first units and shows low amplitude horizontal to sub-horizontal discontinuous reflections. Reflections located below HAT level (covering unit 2) seem more continuous than those located above HAT level. Unit 4 is differentiated from unit 3 by an almost continuous high amplitude horizontal reflection at 7 m IGN. Radar facies of unit 4 is more chaotic than unit 3 facies.

Hook ridge terminus

Profiles D2-03 (Fig. 8C and C') and D2-04 (Fig. 8D and D') are a longitudinal and a cross-section of the investigated hook, respectively. D2-03 is a 60 m long profile from the intersection with D2-02 to the hook terminus [Fig. 8A (I1)]. Signal penetration varies between 7.5 m at the beginning of the profile and about 1.5 m along the thinnest part of the hook. The signal is completely dissipated on a high amplitude continuous and horizontal reflection at 4.5 m IGN, the same elevation of the inter-ridge sandy depression, interpreted as the water table (Fig. 8C). Moderate-amplitude, continuous reflections located below HST level are downlapping on the horizontal basal reflection with an angle of 3°, and up to 9° at their termination (Fig. 8C'). Sequences of downlapping reflections are bounded by erosion surfaces (moderate-amplitude reflections). Unit 1 described in profile D2-02 is intersected in the first 20 m of the profile, between 5 m and 6 m IGN, by a high amplitude reflection with an angle of 1 to 2°. Unit 3 is above this surface and represents a berm facies (Fig. 4, F2). Unit 4, over unit 3, is delimited by two concave and high amplitude reflections at 7 m IGN. This last unit constitutes the top of the main barrier, which reaches 8 m IGN, and is composed of conform and discontinuous reflections.

Profile U2-04 intersects unit 1 perpendicularly at 44 m [Fig. 8C' (I2)]. The profile is 17 m long

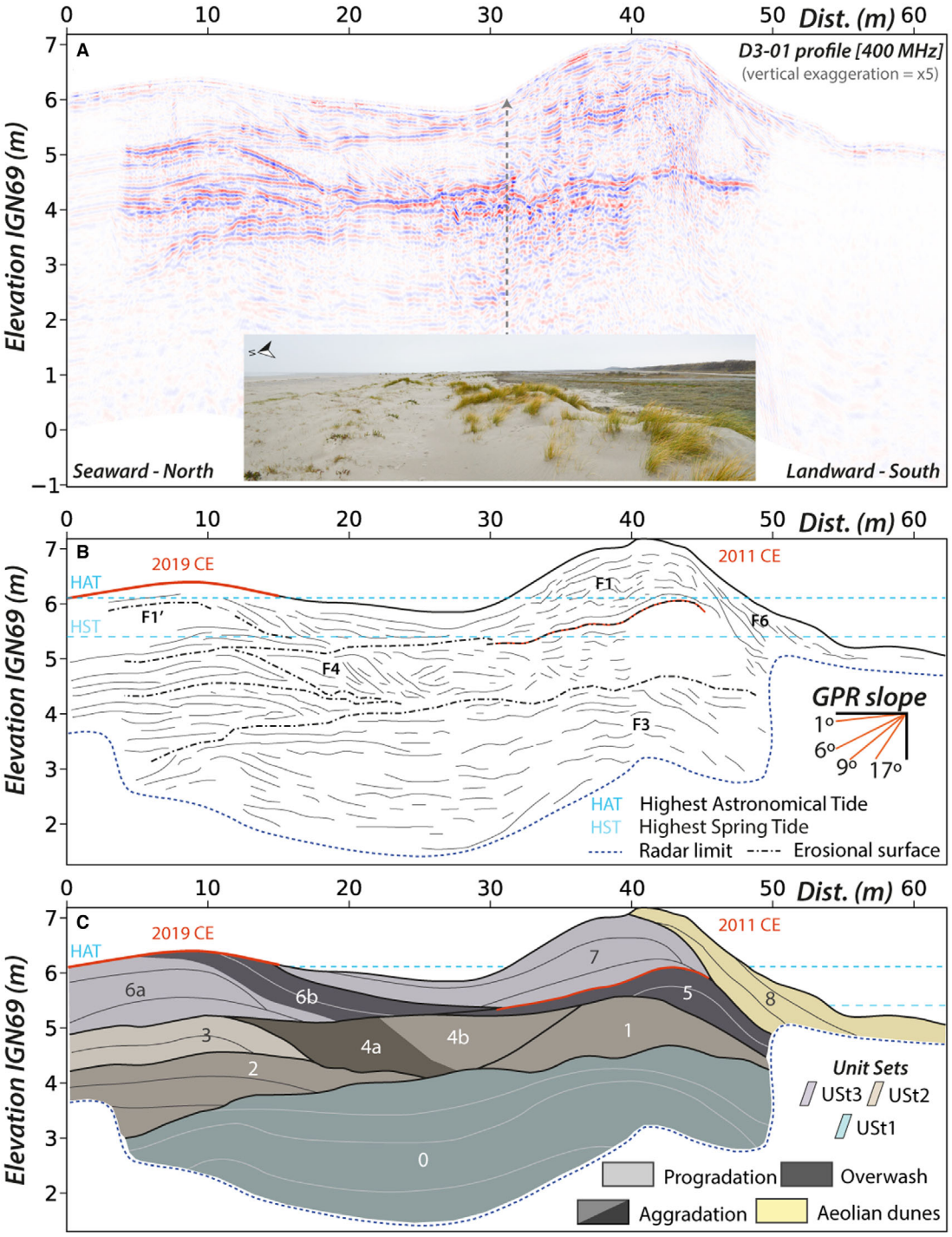

Fig. 7. D3-01 GPR profile interpretation in the spit terminus domain D3. (A) GPR data. (B) Line drawing. (C) Interpretation with unit numbers (sedimentary bodies), stacking pattern and Unit Set numbers (USt).

and shows a maximum signal penetration of 1.5 m down to the water table (Fig. 8D). Unit 1 has been subdivided into four cross-shore sub-units separated by moderate-amplitude and continuous reflections. Unit 1a has a purely aggrading geometry with conforming reflections. Unit 1b is slightly prograding and unit 1c slightly overwashing. Unit 1d overtops the three sub-units and is slightly asymmetrical towards the sea.

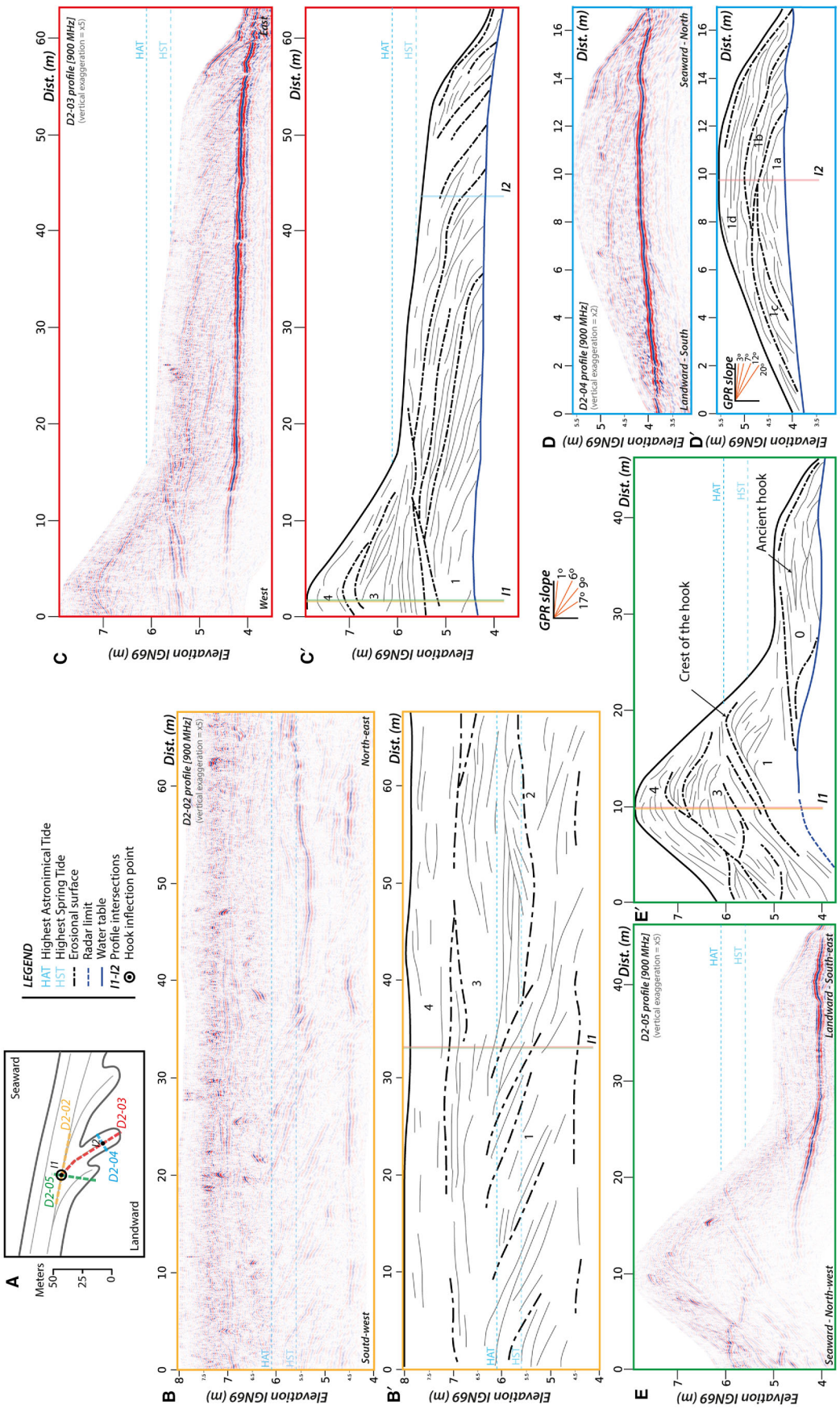

Fig. 8. Interpretation of GPR profiles D2-02 to D2-05 across hooks in the intermediate domain D2. (A) Profile location. (B) to (E) GPR profiles. (B') to (E') Interpreted profiles. I1 and I2: profile intersections.

Inflection point

D2-05 is a 45 m long profile, perpendicular to the main ridge. It crosses profile D2-02 at the ridge inflection point [Fig. 8E' (I1)]. Signal penetration depth is about 3.5 m at the top of the main ridge and decreases to <1 m after 25 m. The main ridge is symmetrical, with seaward and landward slope angles of 10°, and lean on an ancient hook with an almost flat top (Unit 0, Fig. 8E'). The water table, located at an elevation of 4 m IGN and 4.5 m IGN below the main ridge and the fossilized hook, respectively, is identified by a strong reflection which progressively disappears towards the main ridge seaward face. The basal ridge unit (Unit 1, Fig. 8E') shows a typical berm facies (Fig. 4, F3) and its crest reaches an altitude of 6 m IGN. Unit 3 represents another berm, with a crest almost reaching 7 m IGN. Unit 4 is aggrading above unit 3, reaching 8 m IGN, and shows beach-face facies (compare Fig. 4, F1). The position of the ridge crest moved 10 m seaward from unit 1 to 4. According to its position, the basal berm (unit 1) corresponds to a hooked-ridge termination and forms the basement of the inflection point. Units 3 and 4 correspond to a new phase of ridge elongation, and the subsequent abandonment of the hooked terminus.

DISCUSSION

Depositional model for the Mollière spit

Development of individual ridges

Revealing the internal architecture of individual ridges allows proposing a model for their development, comprising two phases (Fig. 9). The first phase is the creation of a ridge core situated below the HAT. This limit is linked to the limit of the breaker zone, where the bedload transport of pebbles by the littoral drift occurs (Carter & Orford, 1993). The longitudinal section of the ridge core is characterized by low-angle sigmoid strata dipping in the direction of the littoral drift (Fig. 8C'); the cross-section is symmetrical (Fig. 8D'). The aggradational architecture of the core is associated with the beach drift in the breaker zone which supplies gravels to the ridge terminus, subsequently reworked by wave refraction. This architecture, with steep landward-dipping strata, is specific to barrier spits, where ridge development is associated with elongation through beach drift, and it does not result from storm activity or berm development as in beach ridge systems (Tamura, 2012; Bendixen *et al.,* 2013; Hein & Ashton, 2020).

The second phase, dominated by cross-shore processes allows the aggradation of the ridge above the HAT level, and is thus assumed to occur during storm-surge events. Corresponding structures are composed of swash deposits on the seaward face of the ridge as well as overtopping and overwashing deposits on its top and back (for example, units 17 and 18, Fig. 6C). Swash deposits generate the steepest strata of the ridge, increasing the initial ridge core slope. Landward-dipping strata associated with overwashing deposits can be as steep as swash deposits if the ridge is isolated. When the ridge is close to or leaning against an older ridge, overwash deposits can form a gently landward-dipping terrace, with strata paralleling the basal surface (for example, units 9 and 13b, Fig. 6C). Similar cross-shore geometries associated with

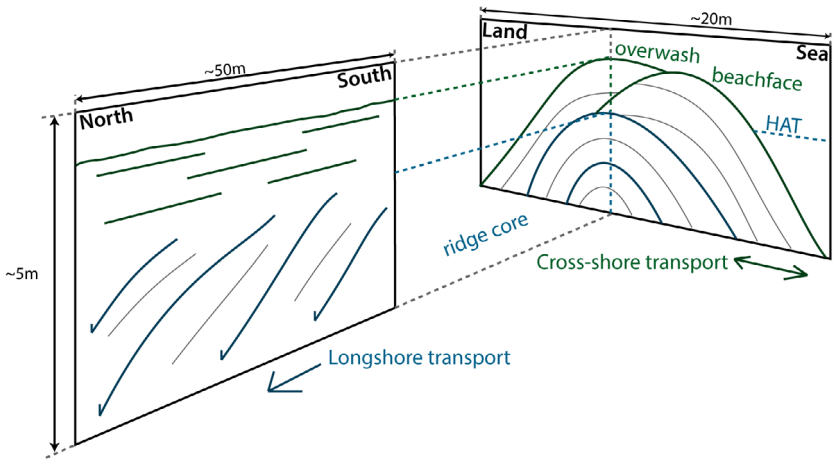

Fig. 9. Model of gravel-ridge development. Two views (longshore and cross-shore sections) of ridge internal structures show beach-face configuration, overwash deposits and ridge core. HAT, Highest Astronomical Tide.

beach-face, overtopping and overwash deposits have been reported by Bennett *et al.* (2009) on the swash-aligned gravel barrier of Chesil Beach (UK). Billy *et al.* (2014) investigated the internal architecture of sand-and-gravel beach ridges on both sides of the Miquelon–Langlade tombolo (north-west Atlantic), with contrasting wave exposures. They found that internal reflectors of ridges formed along the more exposed coast are 1 to 2° steeper than those formed along the more sheltered coast.

The development of individual gravel ridges is thus characterized by a first phase comprising spit elongation by deposition of down-drift dipping strata below the HAT level, and a second phase comprising aggradation associated with swash and overtopping/overwash deposits (Fig. 9). The coincidence between the top elevation of the spit foresets and the highest tide level has been described by Fruergaard *et al.* (2020) in a hypertidal sandy barrier spit. In other systems (e.g. Lindhorst *et al.,* 2008, 2010; Costas & FitzGerald, 2011), this distinction is not observed. The sedimentary structures are continuous across the highest tide level, and the upper beach-face deposits show clear down-drift dipping strata in longitudinal sections.

Hook formation

The combination of GPR data from profiles D2-02 to D2-05 (Fig. 8) with timing derived from image analysis allows proposing a morpho-stratigraphical model of gravel hook formation. This model (Fig. 10) is composed of five morphological steps (1 to 5) associated with four stratigraphical cross-sections (A to D). Step 1 corresponds to the longshore elongation of an individual ridge over the sand platform, with the previously described aggrading core architecture (Fig. 10–A1). Step 2 represents the onshore migration of the ridge terminus, as documented by overwashing geometries that replace the conform and symmetrical ridge core (Fig. 10–B2). This architecture, located at the base of the ridge (Unit 1, Fig. 8E'), may be associated with a storm event or several storm events during high tide levels. During Step 3, the longshore elongation of the ridge terminus, which is now recurved landward (hook morphology), resumes (Fig. 8C) and the overwashing beds are covered by progradational and aggradational geometries that result from longshore transport (Fig. 10–C3, units 3 and 4 in Fig. 8E'). In Step 4, the transport recovers its original shore-parallel direction, and the sand platform re-initiates growth. The welding of swash bars at the hook front probably plays an important role in initiating this new stage of ridge construction through longshore elongation as this can be seen in the intermediate domain between 1982 and 1991 CE (Fig. 3–D2). The sheltered hook is no longer supplied by the littoral drift and becomes abandoned (Fig. 10–D4). The first steps of development of the new ridge are illustrated in B5 and C5 (Fig. 10). In B5, the ridge is prograding and aggrading. In C5, a new ridge can form and lean on the beach face of the initial recurved ridge. The final Step 5 corresponds to the development of the new ridge in front of the abandoned ridge (D5).

The role of swash bars in the development of sandy barrier spits has been studied in some macrotidal inlets (Robin & Levoy, 2007; Robin *et al.,* 2009a, 2009b; Montreuil *et al.,* 2014; Le Bas & Levoy, 2018). These morphologies are integrated into the terminus of the sandy spits (Robin *et al.,* 2009b, 2020) and have even been found in the architecture of some barriers in microtidal (Nielsen & Johannessen, 2009), mesotidal (Lindhorst *et al.,* 2008, 2013; Costas & FitzGerald, 2011) and macrotidal environments (Fruergaard *et al.,* 2020). The role of swash bars in the development of gravel barriers has not been studied yet but they seem to be an important element of gravel spit dynamics. According to this conceptual model, hook formation is thought to be triggered by storm-generated overwashing that amplifies the ridge-terminus curvature, and the following stage of shore-parallel ridge-terminus elongation can be facilitated by the welding of swash bars.

Alongshore evolution of the spit architecture

The Mollière spit shows contrasting morphologies and sedimentary architectures from the spit root to the terminus (Fig. 11). The root of the Mollière spit is located immediately downstream of the fulcrum point of the larger Cayeux spit, which marks the transition from an erosional to an accretional coast (*sensu* Ashton *et al.,* 2016). The root domain (D1) features a characteristic morphology with stacked parallel ridges. It can be seen from aerial photographs (Fig. 3) that individual ridges in D1 grow down-drift under the action of oblique waves. Because of the strong linearity of the coastline at the spit root, and because the sand platform is not well-developed, there is little space available for the new gravel ridges to elongate on the sand flat. Thus, they develop at the foot of pre-existing

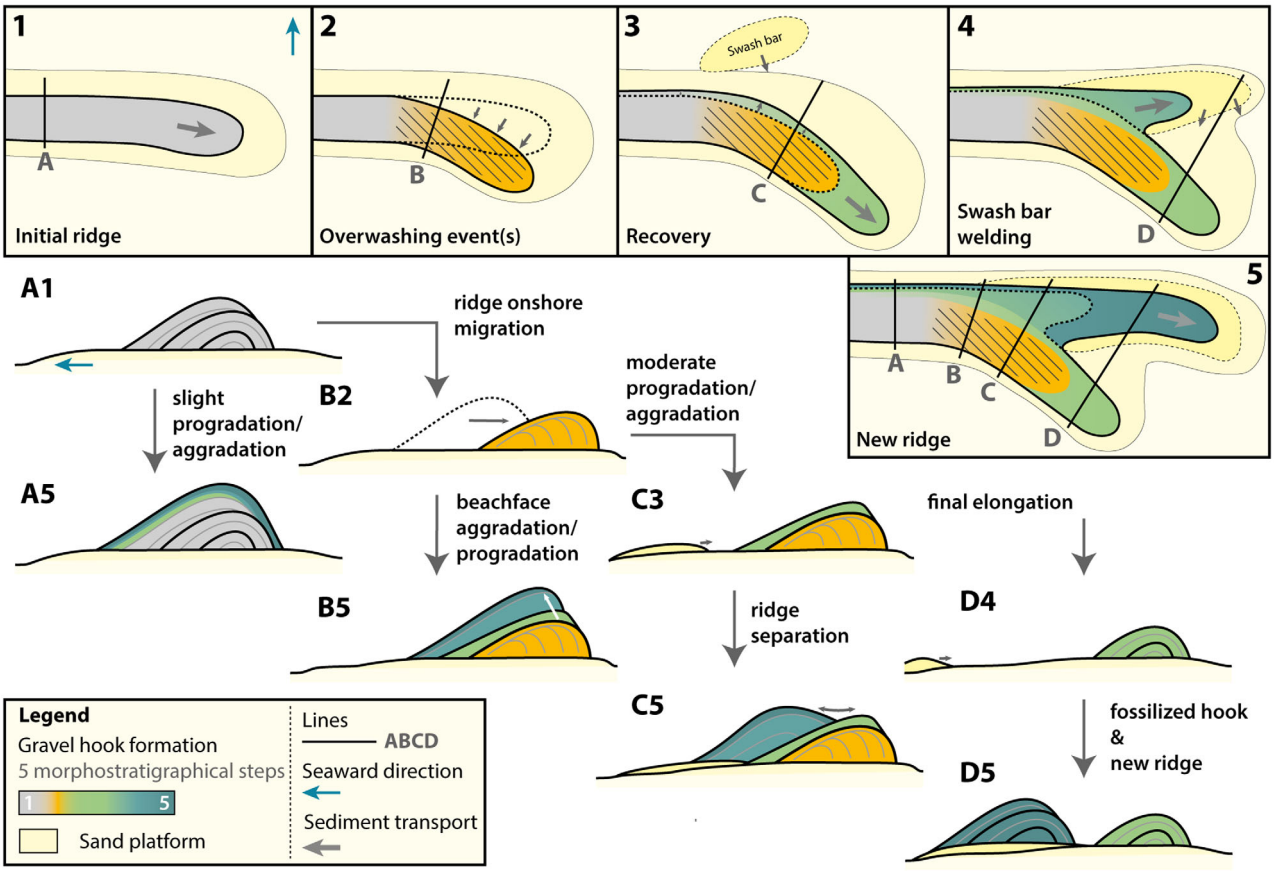

Fig. 10. Principle of hook formation during the evolution of a single ridge.

ridges. Exposed to wave action, the new ridges are reworked and amalgamated to the spit barrier. The internal architecture of the root domain reflects the reworking of individual ridges by cross-shore processes; stacked prograding sequences of well-developed beach-face deposits including large berms and some washover deposits. The resulting architecture has some common characteristics with beach-ridge sequences, as reported by Montes *et al.* (2018) in sandy-to-gravel beach-ridge plain of Río Chico (Argentina). In that model, prograding beach-face sequences are deposited during fair-weather conditions and berm deposits are emplaced during the post-storm recovery of the eroded beach profile through the development and migration of swash bars. On the Mollière spit, it is also clear that berms form on flattened beach-face slopes (2 to 3°), and subsequently contribute to the beach face recovery with much greater slope values. However, there is no evidence from aerial photographs that sandy swash bars can migrate atop the very coarse gravel beach and contribute to the construction of the berm deposits.

In the intermediate domain (D2), individual spit ridges, which correspond to incremental growth of the Mollière spit, are well-preserved. There is, however, an increasing tendency of ridge stacking from Unit Set 1 (USi1) to Unit Set 3 (USi3). This is attributed to the downdrift migration of the Mollière spit and the subsequent straightening of the coastline which reduces the space available for ridge development; the morphology and structure of the intermediate domain are slowly evolving towards those of the root domain. The aggradational geometry of ridge cores is quite unusual in spit systems. Spit ridges and barriers generally experience intense rollover due to storm surge induced washovers, as indicated by high-angle landward dipping stratifications (e.g. Tillmann & Wunderlich, 2013; Montes *et al.*, 2018). Only a few papers, such as those of Smith *et al.* (2003) and Wright *et al.* (2018), reported stacked sequences of convex-shape GPR reflections constituting the core of a fossil coarse-

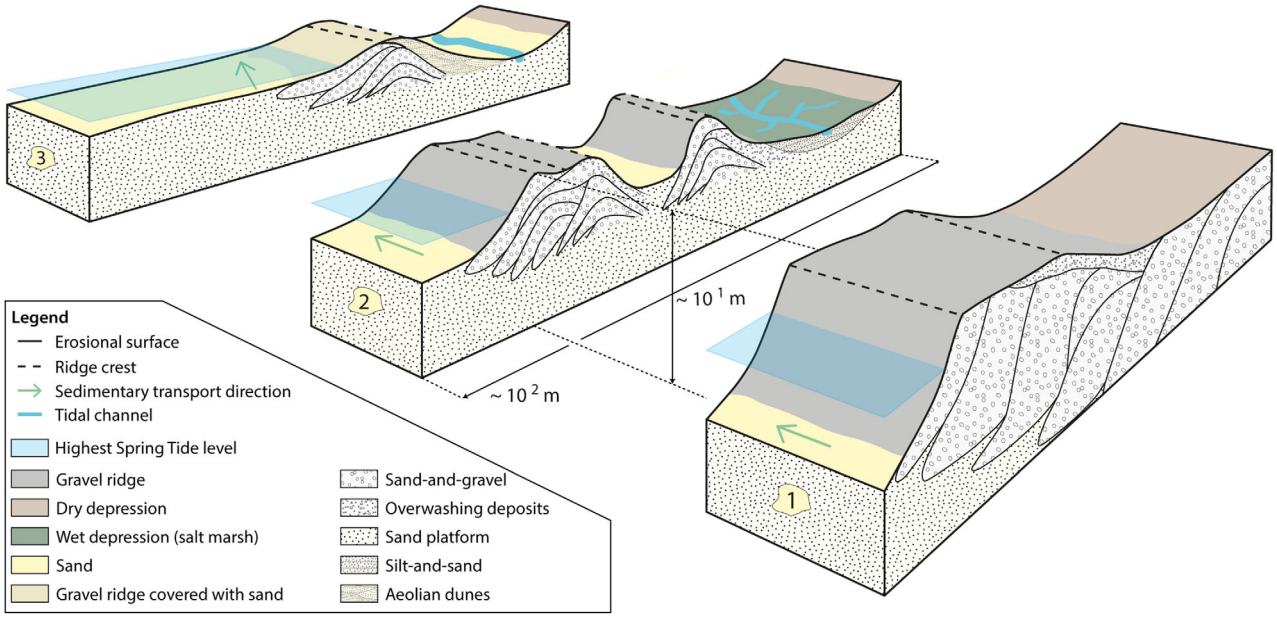

Fig. 11. Morpho-sedimentary structures of the root (D1), intermediate (D2) and terminus (D3) domains of La Mollière gravel spit. For location of the three domains see Fig. 2.

grained spit at Lake Bonneville (Utah, USA) and of a modern sandy spit at Long Bay (South Carolina, USA), respectively. The absence of complete ridge rollover on the Mollière spit is probably due to the rapid elongation of new spit ridges on the shallow sand flat, which protects the older ones from further reworking. Moreover, in a macrotidal environment, the co-occurrence of energetic wave events and HST flooding is rare and of short duration (Robin *et al.,* 2020), thus minimizing the time available for the reworking of spit ridges.

At the spit terminus (D3, Fig. 7), the sand platform plays a significant role in ridge development. Due to the proximity of the ebb-tidal delta of the Somme estuary, the sand platform in front of this part of the spit is wider and has a higher elevation (5 to 6 m IGN) compared with the updrift parts of the spit (morpho-sedimentary domains 1 and 2, 3 to 4 m IGN). The ridges are thus more protected from wave action, with wave energy dissipated on the sandy platform. Despite having a slightly lower thickness (<1 m), ridges are less frequently flooded due to this protection from storm surges. Gravel fluxes to the spit terminus are thus reduced, and the dynamics of swash bars that migrate shoreward on the sand platform supplies sand to the spit. Besides wave action, the wind blowing on the platform during low tide is a significant factor in supplying sand to the barrier. The sand is carried onto the ridges where it settles into the interstitial areas between coarser clasts and contributes to the spit architecture or is deposited on the landward side of the highest ridge creating a dune (Fig. 7C). The high elevation of the sand platform at the Mollière spit terminus is also probably responsible of the planform geometry of the hooked ridges, which feature a relatively small curvature. Based on numerical experiments, Ashton *et al.* (2016) suggested that the depth of the depositional basin controls the length and curvature of the spit hook. In a deeper basin, sediment flux conservation requires a shorter shoreline arc length and larger curvature to prograde the hook with the same rate as in a shallower basin.

The three successive morpho-sedimentary domains are related to the overall longshore development of the spit. During the first stage of development, which may be equivalent to the present-day D3, the littoral drift mainly contributes to the development of individual ridges. As the spit is elongated in the following stages, the fulcrum point migrates downstream (Ashton *et al.,* 2016), increasing sediment by-passing and ridge amalgamation along the upstream domains. The fulcrum point of the Cayeux spit, which was initially located in front of Cayeux-sur-Mer, moves downstream towards the intermediate domain (D2). The root domain (D1) represents

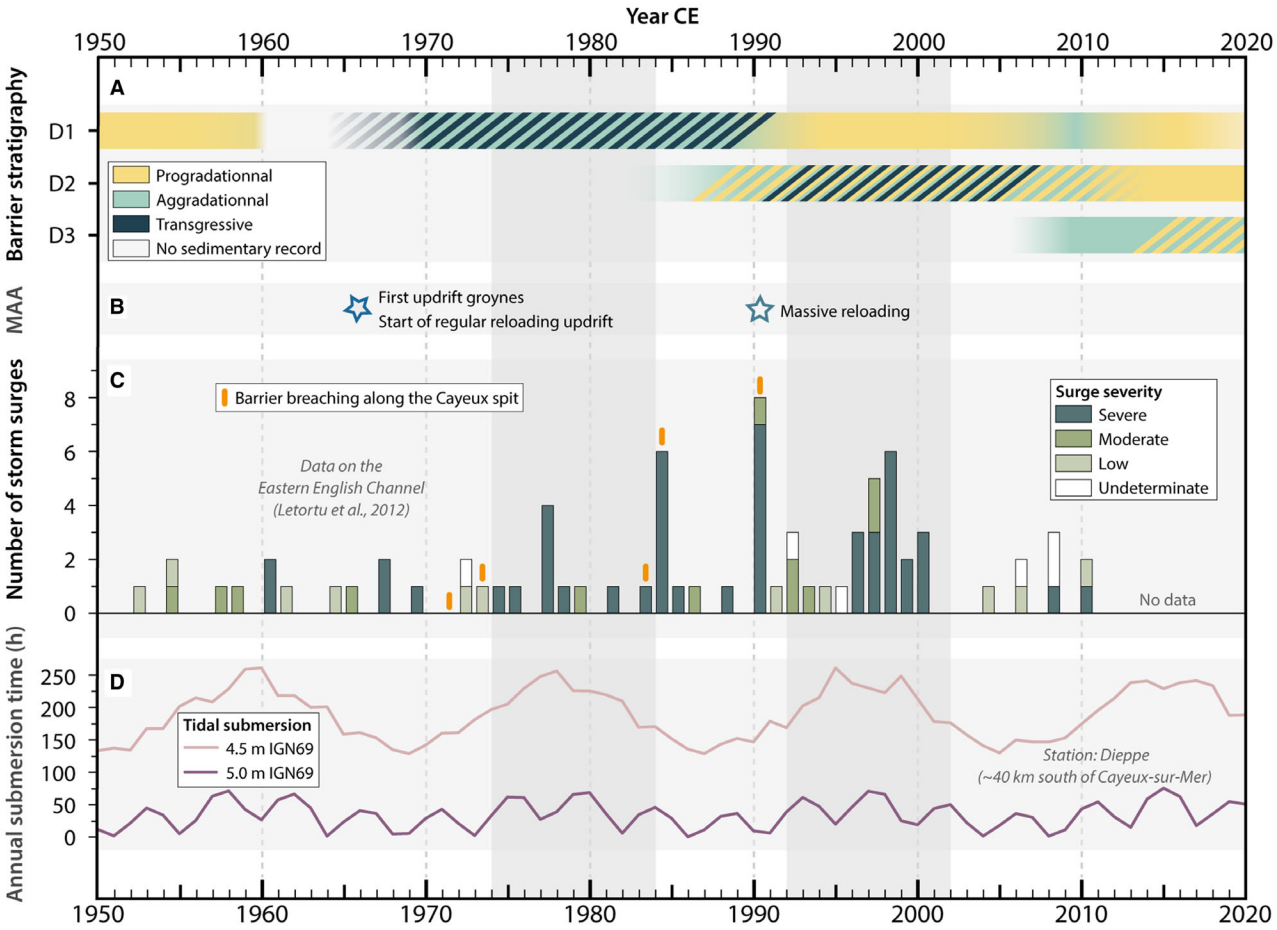

Fig. 12. Barrier spit stratigraphy compared to anthropogenic, climatic and tidal forcings from 1950 CE onward. (A) Evolution of the barrier stratigraphy in the three morpho-sedimentary domains (spit root – D1, intermediate domain – D2, spit terminus – D3; location on Fig. 2). (B) Main anthropogenic actions. (C) Number and severity of historical storm-surge induced submersions in the Eastern English Channel (Letortu *et al.*, 2012). (D) Cumulated annual time of submersion exceeding 4.5 m IGN and 5 m IGN calculated with predicted tide-level data for Dieppe, 40 km south-west of Cayeux-sur-Mer (SHOM, Service Hydrographique et Océanographique de la Marine). Grey bars highlight the periods combining high annual tidal-induced submersion time and intense storm activity.

the most mature evolution of the spit and the remnants of earlier 'downdrift' stages cannot be observed in the GPR profiles. It is possible to characterize a fulcrum 'area' where the progradational beach-face geometries reflect the sediment by-passing towards the downdrift domain. In the terminus domain (D3), the littoral drift is active only during high-tide levels and the spit elongation is slow.

Climatic and anthropogenic control of spit evolution

The temporal evolution of the Mollière spit is characterized by alternating phases of beach-face progradation and erosion, and major periods of barrier retreat with associated transgressive and aggrading deposits (Fig. 12A). The number and length of hooked ridges also seem to vary in time (Fig. 2). It thus might be tempting to identify the major controls of spit evolution.

At the scale of several decades (i.e. the development of the Mollière spit), the evolution of barrier spits is the result of complex interactions between wave and tide dynamics (Allard *et al.*, 2008; Lindhorst *et al.*, 2008; Nielsen & Johannessen, 2009; Poirier *et al.*, 2017), storm impacts (Orford *et al.*, 2002; Fruergaard *et al.*, 2013; Goslin & Clemmensen, 2017) and sediment supply (Allard *et al.*, 2008; Vieira da Silva *et al.*, 2016; Oliver *et al.*, 2017).

The sediment supplied to the Cayeux spit originates from the erosion of chalk cliffs containing flint. The construction of harbour jetties at the end of the 19th century and of two nuclear plants in 1978 CE and 1981 CE has divided the coastline into independent hydro-sedimentary cells, which drastically reduced the gravel flux to the Cayeux spit root (Ault-Onival), from 25 000 m^3 $year^{-1}$ to 2000 m^3 $year^{-1}$ (Leconte & Viguier, 1996). The gravel (D > 20 mm) flux at the Mollière spit root (Cayeux-sur-Mer) is estimated at 80 000 m^3 $year^{-1}$, which results in intense erosion of the Cayeux spit updrift of the fulcrum point (between Ault-Onival and Cayeux-sur-Mer). As a result of this erosion, two measures have been undertaken: (i) the progressive emplacement of 100 groynes every 90 m from Ault-Onival to Cayeux-sur-Mer since 1965 CE (Fig. 12B), with the aim of slowing down littoral drift in the eroding sector of the Cayeux spit; and (ii) the regular nourishment of the spit with gravels at Ault-Onival (30 000 m^3 $year^{-1}$) and south of Cayeux-sur-Mer (75 000 m^3 $year^{-1}$), together with exceptional nourishment following catastrophic erosion events (for example, 660 000 m^3 $year^{-1}$ in three years after the 1990 CE storm) and for the filling of new groyne fields. Finally, well-rounded gravels are extracted directly on the beach-face for industrial purposes along the Mollière root at a rate of 20 000 m^3 $year^{-1}$. It is clear that the sediment flux to the Mollière spit is strongly controlled by human activities and is variable in time. Also, it is very likely that exceptional beach nourishment updrift of Cayeux-sur-Mer produces pulses of sediment that lead to beach-face progradation and ridge elongation, with a lagged response difficult to estimate.

Storm-related submersion events from 1949 to 2010 CE along the coast of the Eastern English Channel have been studied by Letortu *et al.* (2012) (Fig. 12C). A succession of severe storm surges associated with HST levels occurred from the middle of the 1970s until around 2000 CE, with the most severe events in 1984 CE and 1990 CE, and a cluster from 1935 to 2001 CE (Fig. 12C) (Costa, 1997; Bastide *et al.,* 2007; Letortu *et al.,* 2012). Along the Cayeux spit, damages due to barrier breaching have been reported regularly since the 14th century, and during the development of the Mollière spit (1935 CE, 1941 CE, 1972 CE, 1974 CE, 1984 CE, 1985 CE and 1990 CE). Evidence of severe storm-induced erosion of the spit barrier are visible on GPR line D1-01 (Fig. 5), where Unit Set 2, deposited between 1952 CE and 1991 CE, features large washover deposits.

Beyond the temporal variability in timing of wave energy, the potential of beach sediment reworking by waves in a macrotidal environment is strongly related to the duration of tidal flooding at the elevation of the gravel ridges (above 4 m IGN at the study site). Prediction-based, tide-related, cumulated annual submersion time (Weill *et al.,* 2013) above 4.5 m IGN oscillates between 125 h and 250 h, and suggests an 18.6 year nodal tidal cycle (Haigh *et al.,* 2011; Peng *et al.,* 2019). The 5 m IGN threshold shows the expression of the 4.4 year tidal cycle (Ray & Merrifield, 2019), with variation of the annual cumulated submersion time between 0 h and 70 h (Fig. 12D). These significant variations of the potential of sediment reworking by waves may affect the development and migration of swash bars on the upper tidal flat, and the longshore gravel fluxes on the ridges during fairweather conditions.

The relative contributions of the different controls of spit evolution remain very difficult to untangle, in this particular context of a macrotidal environment heavily impacted by coastal management. This is without considering the autogenic feedbacks (e.g. Cooper *et al.,* 2007; Chaumillon *et al.,* 2014), potentially producing autocyclic signals in the spit morphology and dynamics.

CONCLUSION

In this study, the internal architecture of the Mollière gravel spit in the Baie de Somme has been investigated and correlated with its morphological evolution since the 1940s.

Radar facies and surfaces were analysed and interpreted in terms of progradational, aggradational and transgressive depositional units, which helped to develop a depositional and architectural model for this coarse-grained coastal barrier. The spit can be divided into three main morpho-sedimentary domains. The first domain (D1), located at the spit root, shows aggradational and progradational structures which are mainly associated with the cross-shore dynamics. For the intermediate domain (D2), the internal architecture reveals the predominance of structures related to the longshore dynamics below the highest tide level, associated with elongation of new ridges. Sedimentary structures above the highest tide level reflect cross-shore dynamics. The architecture of

the terminus domain (D3) also reflects the longshore dynamics with aggradational and progradational structures but is also significantly influenced by the proximity of the ebb-tidal delta of the Somme estuary, the sandbanks and the development of swash bars.

The internal structure of a spit hook and of a divergence point between two individual ridges has been surveyed in detail. It is suggested that the process of ridge curving (creation of a hook) is triggered by storm-generated overwashing. The subsequent stage of hooked ridge abandonment and the growth and elongation of a new ridge can be facilitated by the attachment of swash bars.

The temporal evolution of the barrier stratigraphy has been compared with human activities, submersion frequency and duration of tidal inundation during the period of spit growth. The relative contributions of the different controls of spit evolution are very difficult to untangle in this context of macrotidal and managed environment. However, severe storms are clearly related to transgressive units described in the ground penetrating radar (GPR) profiles, and abundant beach nourishment after barrier breaching is probably responsible for pulses of spit-ridge elongation. Finally, the tidal modulation of wave activity through submersion time is significant and may play a role in barrier dynamics. Future work has now to be undertaken to understand how this decennial-scale spit dynamics integrates within the long-term evolution and stratigraphy of the main barrier.

ACKNOWLEDGEMENTS

This study is based on the doctoral work of L. Pancrazzi, funded by the French Ministry of Higher Education, Research and Innovation, and financially supported by the French National program EC2CO (CNRS-INSU) and the "Agence de l'Eau Artois-Picardie". Olivier Monfort provided essential support for the DGPS data processing. Finally, we are very grateful to the three anonymous reviewers, as well as to the Associate Editor, John Patrick Walsh, for their very detailed reviews and constructive comments that greatly helped to improve this paper.

DATA AVAILABILITY STATEMENT

Data sharing is not applicable to this article as no new data were created or analyzed in this study.

REFERENCES

Allard, J., **Bertin, X.**, **Chaumillon, E.** and **Pouget, F.** (2008) Sand spit rhythmic development: a potential record of wave climate variations? Arçay spit, western coast of France. *Mar. Geol.*, **253**, 107–131.

Anthony, E.J. (2002) Long-term marine bedload segregation, and sandy versus gravelly Holocene shorelines in the eastern English Channel. *Mar. Geol.*, **187**, 221–234.

Archer, A.W. (2013) World's highest tides: hypertidal coastal systems in North America, South America and Europe. *Sed. Geol.*, **284**, 1–25.

Ashton, A.D., **Nienhuis, J.** and **Ells, K.** (2016) On a neck, on a spit: controls on the shape of free spits. *Earth Surf. Dyn.*, **4**, 193–210.

Bastide, J. (2011) Morphodynamique et enjeux d'aménagement des franges littorales d'un estuaire macrotidal tempéré: La Baie de Somme, Picardie, France. PhD Thesis, University of Littoral Côte d'Opale, 332 p.

Bastide, J., **Anthony, E.J.** and **Dolique, F.** (2007) Le littoral des Bas-Champs soumis aux risques perpétuels d'inondation. IAHS-AISH publication, 211–223.

Baumann, J., **Chaumillon, E.**, **Bertin, X.**, **Schneider, J.L.**, **Guillot, B.** and **Schmutz, M.** (2017) Importance of infragravity waves for the generation of washover deposits. *Mar. Geol.*, **391**, 20–35.

Bendixen, M., **Clemmensen, L.B.** and **Kroon, A.** (2013) Sandy berm and beach-ridge formation in relation to extreme sea-levels: a Danish example in a micro-tidal environment. *Mar. Geol.*, **344**, 53–64.

Bennett, M.R., **Cassidy, N.J.** and **Pile, J.** (2009) Internal structure of a barrier beach as revealed by ground penetrating radar (GPR): Chesil beach, UK. *Geomorphology*, **104**, 218–229.

Billy, J., **Robin, N.**, **Hein, C.J.**, **Certain, R.** and **FitzGerald, D.M.** (2014) Internal architecture of mixed sand-and-gravel beach ridges: Miquelon-Langlade barrier, NW Atlantic. *Mar. Geol.*, **357**, 53–71.

Buscombe, D. and **Masselink, G.** (2006) Concepts in gravel beach dynamics. *Earth Sci. Rev.*, **79**, 33–52.

Carter, R.W.G. and **Orford, J.D.** (1984) Coarse clastic barrier beaches: a discussion of their distinctive dynamic and morpho-sedimentary characteristics. *Mar. Geol.*, **60**, 377–389.

Carter, R.W.G. and **Orford, J.D.** (1993) The morphodynamics of coarse clastic beaches and barriers: a short and long-term perspective. *J. Coastal Res.*, **15**, 158–179.

Chaumillon, E., **Ozenne, F.**, **Bertin, X.**, **Long, N.** and **Ganthy, F.** (2014) Control of wave climate and meander dynamics on spit breaching and inlet migration. *J. Coast. Res.*, **70**, 109–114.

Colbeaux, J.P., **Dupuis, C.**, **Robaszinski, F.**, **Auffret, J.P.**, **Haesazaerts, P.** and **Somme, J.** (1980) Le détroit du Pas de Calais un élément dans la tectonique de blocs de l'Europe nord-occidentale. *Bull. Inf. Géol. Bass. Paris*, **4**, 41–54.

Cooper, J.A.G., **McKenna, J.**, **Jackson, D.W.T.** and **O'connor, M.** (2007) Mesoscale coastal behavior related to morphological self-adjustment. *Geology*, **35**, 187–190.

Costa, S. (1997) "Dynamique littorale et risques naturels": L'impact des aménagements, des variations du niveau marin et des modifications climatiques entre la Baie de Seine et la Baie de Somme (Haute-Normandie, Picardie; France). PhD Thesis, University of Paris 1, 343 p.

Costas, S. and **FitzGerald, D.** (2011) Sedimentary architecture of a spit-end (Salisbury Beach,

Massachusetts): the imprints of sea-level rise and inlet dynamics. *Mar. Geol.*, **284**, 203–216.

Davidson-Arnott, R.G. and **Fisher, J.D.** (1992) Spatial and temporal controls on overwash occurrence on a Great Lakes barrier spit. *Can. J. Earth Sci.*, **29**, 102–117.

Dolique, F. and **Anthony, E.J.** (1999) Influence à moyen terme (10-100 ans) d'un estran sableux macrotidal sur la stabilité d'un cordon de galets: la flèche de Cayeux (Picardie, France). *Géomorphol. Relief Process. Environ.*, **5**, 23–38.

Dubar, M. and **Anthony, E.J.** (1995) Holocene environmental change and river-mouth sedimentation in the Baie des Anges French Riviera. *Quatern. Res.*, **43**, 329–343.

Dupont, J.-P. (1981) Relations entre bios et phénomènes sédimentaires intertidaux: le modèle de la Baie de Somme. PhD Thesis, University of Rouen Normandie, 310 p.

Engels, S. and **Roberts, M.C.** (2005) The architecture of prograding sandy-gravel beach ridges formed during the last holocene highstand: southwestern British Columbia, Canada. *J. Sed. Res.*, **75**, 1052–1064.

Etienne, S. and **Terry, J.P.** (2012) Coral boulders, gravel tongues and sandd sheets: features of coastal accretion and sediment nourishment by cyclone Tomas (march 2010) on Taveuni Island, Fiji. *Geomorphology*, **175**, 54–65.

Forbes, D.L., **Orford, J.D.**, **Carter, R.W.G.**, **Shaw, J.** and **Jennings, S.C.** (1995) Morphodynamic evolution, self-organisation, and instability of coarse-clastic barriers on paraglacial coasts. *Mar. Geol.*, **126**, 63–85.

Fruergaard, M., **Andersen, T.J.**, **Johannessen, P.N.**, **Nielsen, L.H.** and **Pejrup, M.** (2013) Major coastal impact induced by a 1000-year storm event. *Sci. Rep.*, **3**, 1–7.

Fruergaard, M., **Møller, I.**, **Johannessen, P.N.**, **Nielsen, L.H.**, **Andersen, T.J.**, **Nielsen, L.**, **Sander, L.** and **Pejrup, M.** (2015) Stratigraphy, evolution, and controls of a holocene transgressive–regressive barrier Island under changing sea level : Danish North Sea coast. *J. Sed. Res.*, **85**, 820–844.

Fruergaard, M., **Tessier, B.**, **Poirier, C.**, **Mouazé, D.**, **Weill, P.** and **Noël, S.** (2020) Depositional controls on a hypertidal barrier-spit system architecture and evolution, pointe du banc spit, North-Western France. *Sedimentology*, **67**, 502–533.

Goslin, J. and **Clemmensen, L.B.** (2017) Proxy record of Holocene storm events in coastal barrier systems. Storm-wave induced markers. *Quatern. Sci. Rev.*, **174**, 80–119.

Haigh, I.D., **Eliot, M.** and **Pattiaratchi, C.** (2011) Global influences of the 18.61 year nodal cycle and 8.85 year cycle of lunar perigee on high tidal levels. *J. Geophys. Res. Oceans*, **116**, C06025.

Hayes, M.O. (1975) Morphology of sand accumulation in estuaries. In: *Estuarine Research, Vol. 2, Geology and Engineering* (Ed Cronin, L.E.), pp. 3–22. Academic Press, New York, NY.

Hein, C.J. and **Ashton, A.D.** (2020) Long-term shoreline morphodynamics: processes and preservation of environmental signals. In: *Sandy Beach Morphodynamics* (Eds Jackson, D.W.T. and Short, A.D.), pp. 487–531. Elsevier, Amsterdam.

Hine, A.C. (1979) Mechanisms of berm development and resulting beach growth along a barrier spit complex. *Sedimentology*, **26**, 333–351.

Holmes, K.E., **Edinger, E.N.**, **Limmon, G.V.** and **Risk, M.J.** (2000) Bioerosion of live massive corrals and branching coral rubble on Indonesian coral reefs. *Mar. Pollut. Bull.*, **40**, 606–617.

Isla, F.I. and **Bujalesky, G.G.** (2000) Cannibalisation of Holocene gravel beach-ridge plains, northern Tierra del Fuego, Argentina. *Mar. Geol.*, **170**, 105–122.

Jahnert, R., **de Paula, O.**, **Collins, L.**, **Strobach, E.** and **Pevzner, R.** (2012) Evolution of a coquina barrier in Shark Bay, Australia by GPR imaging: architecture of a holocene reservoir analog. *Sediment. Geol.*, **281**, 59–74.

Jennings, R. and **Shulmeister, J.** (2002) A field based classification scheme for gravel beaches. *Mar. Geol.*, **186**, 211–228.

Jol, H.M., **Smith, D.G.** and **Meyers, R.A.** (1996) Digital ground penetrating radar (GPR): a new geophysical tool for coastal barrier research (examples from the Atlantic, gulf and Pacific coasts, USA). *J. Coast. Res.*, **12**, 960–968.

Jol, H.M. and **Bristow, C.** (2003) GPR in sediments: advice on data collection, basic processingand interpretation. A good practice guide. In: *Ground Penetrating Radar in Sediments* (Eds Bristow, C. and Jol, H.M.), Vol. **211**, pp. 9–27. Geological Society. Special Publication, London.

Kirk, R.M. (1975) Aspects of runup processes on mixed sand and gravel beaches. *Geogr. Ann. Ser. A Phys. Geogr.*, **57**, 117–133.

Kulkarni, C.D., **Levoy, F.**, **Monfort, O.** and **Miles, J.** (2004) Morphological variations of a mixed sediment beachface (Teignmouth, UK). *Cont. Shelf Res.*, **24**, 1203–1218.

Le Bas, X.P. and **Levoy, F.** (2018) Bar migrations on a macrotidal Ebb Delta over a period of six years using Lidar survey. *J. Coast. Res.*, **85**, 146–150.

Leatherman, S.P. (1987) Coastal geomorphological applications of ground-penetrating radar. *J. Coast. Res.*, **3**, 397–399.

Leconte, G. and **Viguier, J.** (1996) Protection du littoral des Bas-Champs. *Journées Nationales Génie Côtier - Génie Civil, Paralia*, **4**, 225–236.

Letortu, P., **Costa, S.** and **Cantat, O.** (2012) Les submersions marines en Manche orientale : approche inductive et naturaliste pour la caractérisation des facteurs responsables des inondations par la mer. *Climatologie*, **9**, 31–57.

Letortu, P., **Costa, S.**, **Maquaire, O.**, **Delacourt, C.**, **Augereau, E.**, **Davidson, R.**, **Suanez, S.** and **Nabucet, J.** (2015) Retreat rates, modalities and agents responsible for erosion along the coastal chalk cliffs of upper Normandy: the contribution of terrestrial laser scanning. *Geomorphology*, **245**, 3–14.

Le Xuan, H., **Hanson, H.**, **Larson, M.** and **Kato, S.** (2011) A mathematical model of spit growth and barrier elongation: application to Fire Island inlet (USA) and Badreveln spit (Sweden). *Estuar. Coast. Shelf Sci.*, **93**, 468–477.

Lindhorst, S., **Betzler, C.** and **Hass, H.C.** (2008) The sedimentary architecture of a Holocene barrier spit (Sylt, German bight): swash-bar accretion and storm erosion. *Sed. Geol.*, **206**, 1–16.

Lindhorst, S., **Fuerstenau, J.**, **Christian Hass, H.** and **Betzler, C.** (2010) Anatomy and sedimentary model of a hooked spit (Sylt, southern North Sea). *Sedimentology*, **57**, 935–955.

Lindhorst, S., **Betzler, C.** and **Hass, H.C.** (2013) Large scale architecture of a stacked Holocene spit–the stratigraphy of northern Sylt (southern North Sea) [Großmaßstäbliche Architektur eines holozänen Nehrungshakens–die Stratigrafie von Nord-Sylt (südliche Nordsee).]. *Z. Dtsch. Ges. Geowiss.*, **164**, 63–79.

Lindhorst, S. and **Schutter, I.** (2014) Polar gravel beach-ridge systems: sedimentary architecture, genesis, and implications for climate reconstructions (South Shetland

Islands/Western Antarctic peninsula). *Geomorphology*, **221**, 187–203.

Massari, F. and **Parea, G.C.** (1988) Progradational gravel beach sequences in a moderate-to high-energy, microtidal marine environment. *Sedimentology*, **35**, 881–913.

Michel, C. (2016) Morphodynamique et transferts sédimentaires au sein d'une baie mégatidale en comblement (Baie de Somme, Manche Est). Stratégie multi-échelles spatio-temporelles. PhD Thesis, Normandie University, 502 p.

Michel, C., **Le Bot, S.**, **Druine, F.**, **Costa, S.**, **Levoy, F.**, **Dubrulle-Brunaud, C.** and **Lafite, R.** (2017) Stages of sedimentary infilling in a hypertidal bay using a combination of sedimentological, morphological and dynamic criteria (bay of Somme, France). *J. Maps*, **13**, 858–865.

Montes, A., **Bujalesky, G.G.** and **Paredes, J.M.** (2018) Geomorphology and internal architecture of Holocene sandy-gravel beach ridge plain and barrier spits at Río Chico area, Tierra del Fuego, Argentina. *J. S. Am. Earth Sci.*, **84**, 172–183.

Montreuil, A.L., **Levoy, F.**, **Bretel, P.** and **Anthony, E.J.** (2014) Morphological diversity and complex sediment recirculation on the ebb delta of a macrotidal inlet (Normandy, France): a multiple LiDAR dataset approach. *Geomorphology*, **219**, 114–125.

Neal, A. (2004) Ground-penetrating radar and its use in sedimentology: principles, problems and progress. *Earth Sci. Rev.*, **66**, 261–330.

Neal, A. and **Roberts, C.L.** (2000) Applications of ground-penetrating radar (GPR) to sedimentological, geomorphological and geoarchaeological studies in coastal environments. *Geol. Soc. Lond. Spec. Publ.*, **175**, 139–171.

Neal, A., **Pontee, N.I.**, **Pye, K.** and **Richards, J.** (2002) Internal structure of mixed-sand-and-gravel beach deposits revealed using ground-penetrating radar. *Sedimentology*, **49**, 789–804.

Nielsen, L.H. and **Johannessen, P.N.** (2009) Facies architecture and depositional processes of the Holocene–Recent accretionary forced regressive Skagen spit system, Denmark. *Sedimentology*, **56**, 935–968.

Oliver, T.S., **Donaldson, P.**, **Sharples, C.**, **Roach, M.** and **Woodroffe, C.D.** (2017) Punctuated progradation of the seven Mile Beach Holocene barrier system, southeastern Tasmania. *Mar. Geol.*, **386**, 76–87.

Orford, J.D. and **Anthony, E.J.** (2011) Extreme events and the morphodynamics of gravel-dominated coastal barriers: strengthening uncertain ground. *Mar. Geol.*, **290**, 41–45.

Orford, J.D. and **Carter, R.W.G.** (1982) Crestal overtop and washover sedimentation on a fringing sandy gravel barrier coast, Carnsore point, Southeast Ireland. *J. Sed. Res.*, **52**, 265–278.

Orford, J.D., **Carter, R.W.G.** and **Jennings, S.C.** (1991) Coarse clastic barrier environments: evolution and implications fort Quaternary Sea level interpretation. *Quat. Int.*, **9**, 87–104.

Orford, J.D., **Forbes, D.L.** and **Jennings, S.C.** (2002) Organisational controls, typologies and timescales of paraglacial gravel-dominated coastal systems. *Geomorphology*, **48**, 51–85.

Otvos, E.G. (2012) Coastal barriers – nomenclature, processes, and classification issues. *Geomorphology*, **139**, 39–52.

Payo, A., **Walkden, M.**, **Ellis, M.A.**, **Barkwith, A.**, **Favis-Morttlock, D.**, **Kessler, H.**, **Wood, B.**, **Burke, H.** and **Lee, J.** (2018) A quantitative assessment of the annual contribution of platform downwearing to beach sediment budget: Happisburgh, England, UK. *J. Mar. Sci. Eng.*, **6**, 113.

Peng, D., **Hill, E.M.**, **Meltzner, A.J.** and **Switzer, A.D.** (2019) Tide gauge records show that the 18.61-year nodal tidal cycle can change high water levels by up to 30 cm. *J. Geophys. Res. Oceans*, **124**, 736–749.

Plattner, A.M. (2020) GPRPy: open-source ground-penetrating radar processing and visualization software. *Lead. Edge*, **39**, 332–337.

Poirier, C., **Tessier, B.**, **Chaumillon, E.**, **Bertin, X.**, **Fruergaard, M.**, **Mouazé, D.**, **Weill, P.** and **Wöppelmann, G.** (2017) Decadal changes in North Atlantic atmospheric circulation patterns recorded by sand spits since 1800 CE. *Geomorphology*, **281**, 1–12.

QGIS Development Team (2019) QGIS Geographic Information System. QGIS Association. http://www.qgis.org

Ray, R.D. and **Merrifield, M.A.** (2019) The semiannual and 4.4-year modulations of extreme high tides. *J. Geophys. Res. Oceans*, **124**, 5907–5922.

Robin, N. and **Levoy, F.** (2007) Etapes et rythmes de formation d'une flèche sédimentaire à crochets multiples en environnement mégatidal. *Z. Geomorphol.*, **51**, 337–360.

Robin, N., **Levoy, F.** and **Monfort, O.** (2009a) Short term morphodynamics of an intertidal bar on megatidal ebb delta. *Mar. Geol.*, **260**, 102–120.

Robin, N., **Levoy, F.**, **Monfort, O.** and **Anthony, E.** (2009b) Short-term to decadal-scale onshore bar migration and shoreline changes in the vicinity of a megatidal ebb delta. *Case Rep. Med.*, **114**, F04024.

Robin, N., **Levoy, F.**, **Anthony, E.J.** and **Monfort, O.** (2020) Sand spit dynamics in a large tidal-range environment: insight from multiple LiDAR, UAV and hydrodynamic measurements on multiple spit hook development, breaching, reconstruction, and shoreline changes. *Earth Surf. Proc. Land.*, **45**, 2706–2726.

SHOM (2017) Références Altimétrique Maritimes. Port de France métropolitaine et d'outre-mer. Cotes du zéro hydrographique et niveaux caractéristiques de la marée. 118 p.

Smith, D.G., **Simpson, C.J.**, **Jol, H.M.**, **Meyers, R.A.** and **Currey, D.R.** (2003) GPR stratigraphy used to infer transgressive deposition of spits and a barrier, Lake Bonneville, Stockton, Utah, USA. In: *Ground Penetrating Radar in Sediments* (Eds Bristow, C. and Jol, H.M.), Vol. **211**, pp. 79–86. Geological Society. Special Publications, London.

SOGREAH (1995) Etude sédimentologique de la Baie de Somme. Synthèse des données naturelles. Rapport, Direction Départementale de l'Equipement de la Somme, Abbeville, France, 65p.

Tamura, T., **Murakami, F.**, **Nanayama, F.**, **Watanabe, K.** and **Saito, Y.** (2008) Ground-penetrating radar profiles of Holocene raised-beach deposits in the Kujukuri strand plain, Pacific coast of eastern Japan. *Mar. Geol.*, **248**, 11–27.

Tamura, T. (2012) Beach ridges and prograded beach deposits as palaeoenvironment records. *Earth Sci. Rev.*, **114**, 279–297.

Tillmann, T. and **Wunderlich, J.** (2013) Barrier rollover and spit accretion due to the combined action of storm surge induced washover events and progradation: insights from ground-penetrating radar surveys and sedimentological data. *J. Coastal Res.*, **65**, 600–605.

Tye, R.S. and **Moslow, T.F.** (1993) Tidal inlet reservoirs: insights from modern examples. In: *Marine Clastic*

Reservoirs. Frontiers in Sedimentary Geology (Eds Rhodes, E.G. and Moslow, T.F.), pp. 77–99. Springer, New York, NY.

van Heteren, S., **FitzGerald, D.M.**, **Barber, D.C.**, **Kelley, J.T.** and **Belknap, D.F.** (1996) Volumetric analysis of a New England barrier system using ground-penetrating-radar and coring techniques. *J. Geol.*, **104**, 471–483.

van Heteren, S., **Fitzgerald, D.M.**, **McKinlay, P.A.** and **Buynevich, I.V.** (1998) Radar facies of paraglacial barrier systems: coastal New England, USA. *Sedimentology*, **45**, 181–200.

Vieira da Silva, G., **Muler, M.**, **Prado, M.F.V.**, **Short, A.D.**, **Klein, A.H.F.** and **Toldo, E.E., Jr.** (2016) Shoreline change analysis and insight into the sediment transport path along Santa Catarina Island north shore, Brazil. *J. Coastal Res.*, **32**, 863–874.

Weill, P., **Tessier, B.**, **Mouazé, D.**, **Bonnot-Courtois, C.** and **Norgeot, C.** (2012) Shelly cheniers on a modern macrotidalflat (Mont-saint-Michel bay, France) — internal architecture revealed by ground-penetrating radar. *Sed. Geol.*, **279**, 173–186.

Weill, P., **Mouazé, D.** and **Tessier, B.** (2013) Internal architecture and evolution of bioclastic beach ridges in a megatidal chenier plain: field data and wave flume experiment. *Sedimentology*, **60**, 1213–1230.

Wright, E., **Kruse, S.**, **Forman, S.L.** and **Harris, M.S.** (2018) Millennial scale development of a southeastern United States spit. *J. Coastal Res.*, **34**, 255–271.

Manuscript received 8 March 2021; revision accepted 27 April 2022